Is the West Antarctic Ice Sheet Disintegrating?

T. HUGHES

Institute of Polar Studies, The Ohio State University, Columbus, Ohio 43210

Data pertaining to the dynamics and history of the west antarctic ice cover are reviewed and interpreted in terms of a possible inherent instability of the ice cover. A study of published data concerning the past and present ice cover of West Antarctica indicates that during the last few million years the ice sheet has been retreating in stages, each retreat stage being preceded by an advance of comparable duration. Thus disintegration of the west antarctic ice sheet seems to follow the disintegration pattern of other continental ice sheets and may be the last phase of the worldwide Late Cenozoic ice age. At least some of the retreat stages seem to have been rapid enough to be called surges. Stages of advance seem to have temporarily introduced equilibrium conditions, since equilibrium ice sheet surface profiles can be reconstructed from the moraines, etc., and thus mark the stable limits of each advance. Present ice sheet surface profiles along flowlines entering both the Ronne and the Ross ice shelves from Marie Byrd Land are not equilibrium profiles, suggesting that the west antarctic ice sheet is unstable. An analysis of the grounded portion of the west antarctic ice cover indicates that data relating to the surface profile, ice velocity, and the mass balance are all incompatible with an equilibrium ice sheet. Instability seems to be centered in the major ice streams that drain Marie Byrd Land. An analysis of the floating portion of the west antarctic ice cover indicates that basal melting is most pronounced along the Siple Coast of the Ross ice shelf and causes retreat of the grounding line into Marie Byrd Land. Instability seems to be related to sudden retreats of the grounding line.

Beginning with the 1957–1958 International Geophysical Year in Antarctica, traverses over the ice sheet have determined surface mean annual temperature, surface elevation, ice thickness, and snow accumulation for most of the continent. The various ice drainage basins of Antarctica defined by ice flowlines are approximately shown in Figure 1 [*Giovinetto*, 1964; *Budd et al.*, 1970]. The west antarctic ice sheet is the most extensively studied, especially the Ross Sea ice drainage basin, as is shown by the articles in volumes 2 and 16 of the *Antarctic Research Series* published by the American Geophysical Union [*Mellor*, 1964; *Crary*, 1971], the coreholes at Little America 5 and Byrd Station [*Bender and Gow*, 1961; *Crary*, 1961; *Gow et al.*, 1968; *Gow*, 1970; *Johnsen et al.*, 1972], the Ross ice shelf survey (RISS) traverse [*Dorrer et al.*, 1969; *Dorrer*, 1970], the Byrd Station strain net (BSSN) traverse [*Dewart*, 1973; *Whillans*, 1973*a*, *b*; *Brecher*, 1973], the Scott Polar Research Institute–National Science Foundation (SPRI-NSF) radio echo aerial traverses [*Robin et al.*, 1970*a*, *b*; *Evans and Robin*, 1972], and shallow coring in the Ross Sea and the Weddell Sea during various cruises of the U.S.N.S. *Eltanin* and the U.S.C.G.C. *Glacier* [*Fillon*, 1972; *Anderson*, 1972].

Comparing the American Geographical Society 1970 map of Antarctica with the United States Geological Survey 1972 map of the Ross ice shelf suggests that major ice streams can be traced from the grounded ice cover of Marie Byrd Land across the floating ice cover of the Ross ice shelf to the continental shelf of the Ross Sea. This impression is emphasized in Figure 2, which shows ice elevation contours and thick ice regions in Marie Byrd Land, ice thickness contours on the Ross ice shelf, and bathymetry contours in the Ross Sea. Trends of major ice streams are shown as dotted bands, and the pattern of these ice streams is surprisingly well defined. Active ice streams in Marie Byrd Land are revealed by crevasse fields and concave surface profiles along the flow direction and by reduced ice elevation but increased ice thickness across the flow direction. Passive ice streams on the Ross ice shelf are revealed by elongated lobes of thick ice in the flow di-

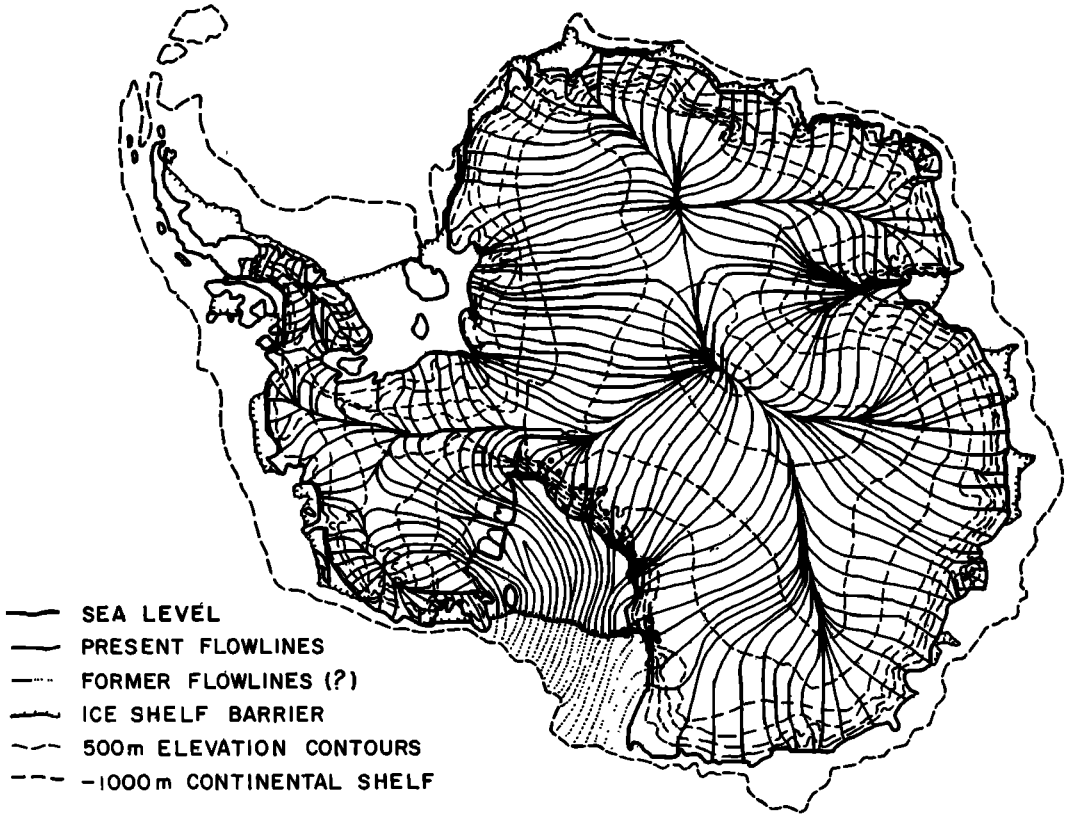

Fig. 1. The distribution of ice flow in Antarctica. Shown are (1) ice flowlines drawn normal to elevation contours, (2) ice drainage basins separated by ice divides, and (3) known deposition sites of the Sirius Formation (solid circles). (Modified from *Budd et al.* [1970] and *Mayewski* [1972].

rection, although flow velocity is remarkably uniform transverse to the flow direction. Former ice streams on the Ross Sea floor are revealed by eroded linear troughs that extend from the Ross ice shelf barrier to the continental shelf, and they seem to match the passive ice stream contours on the ice shelf. The overall impression is that the ice streams are stable features, but their position of grounding is unstable. This would explain their fossil definition on the Ross Sea floor, their passive definition on the Ross ice shelf, and their active definition in Marie Byrd Land.

The Ross Sea ice drainage basin is divided into east antarctic and west antarctic portions by the Transantarctic Mountains, and the latter portion has several features which suggest nonequilibrium flow conditions; specifically, (1) the ice surface is generally concave whereas an equilibrium ice sheet has a convex surface [*Nye*, 1959, 1967; *Haefeli*, 1961; *Weertman*, 1961], (2) evidence of extensive past glaciations is preserved in bordering unglaciated areas and on the Ross Sea floor [*Wade*, 1937; *Doumani*, 1964; *Mercer*, 1968*a*, 1972; *Calkin et al.*, 1970; *Denton et al.*, 1970; *Houtz and Meijer*, 1970; *LeMasurier*, 1972; *Mayewski*, 1972; *Fillon*, 1972], (3) the floating ice cover and possibly the grounded ice cover overlies bedrock that is apparently in isostatic uplift, presumably due to partial reduction of a heavier former ice cover [*Bennett*, 1964; *Robinson*, 1964; *Bentley*, 1964], (4) ice elevations formerly were several hundred meters higher than at present according to oxygen isotope analyses of ice cores at Byrd Station and Little America 5 [*Johnsen et al.*, 1972; Dansgaard, personal communication, 1972], (5) between Byrd Station and the ice

divide, downstream ice output quite possibly exceeds the precipitation ice input, suggesting a negative ice budget in this region [*Whillans*, 1973*a*, *b*; *Brecher*, 1973], (6) a wet base underlies most or all of the grounded ice sheet, which is a necessary but not sufficient condition for a surge of the ice sheet [*Zotikov*, 1963*a*; *Gow et al.*, 1968; *Weertman*, 1969; *Robin et al.*, 1970*b*; *Budd et al.*, 1970; *Dewart*, 1973], and (7) thermal instability may be widespread in the grounded ice cover and might lead to thermal convection [*Hughes*, 1971, 1972*a*, *b*; *Bentley*, 1971] and perhaps surges [*Wilson*, 1964; *Weertman*, 1966; *Hughes*, 1970].

Most of the Ross Sea ice drainage basin terminates in the Ross ice shelf. The major ice streams feeding the Ross ice shelf from the grounded ice cover in East Antarctica and West Antarctica are shown in Figure 2. Three ice streams are of particular interest. Ice stream D approximately parallels the BSSN traverse and is near the only coreholes through the grounded ice cover (at Byrd Station) and the floating ice cover (at Little America 5) of the drainage basin. Ice stream C approximately parallels the Bentley subglacial trench, and intersects the E-W leg (at station 53) and the N-S leg (at station 133) of the RISS traverse. Ice stream A is the approximate boundary between the portions of the Ross ice shelf fed

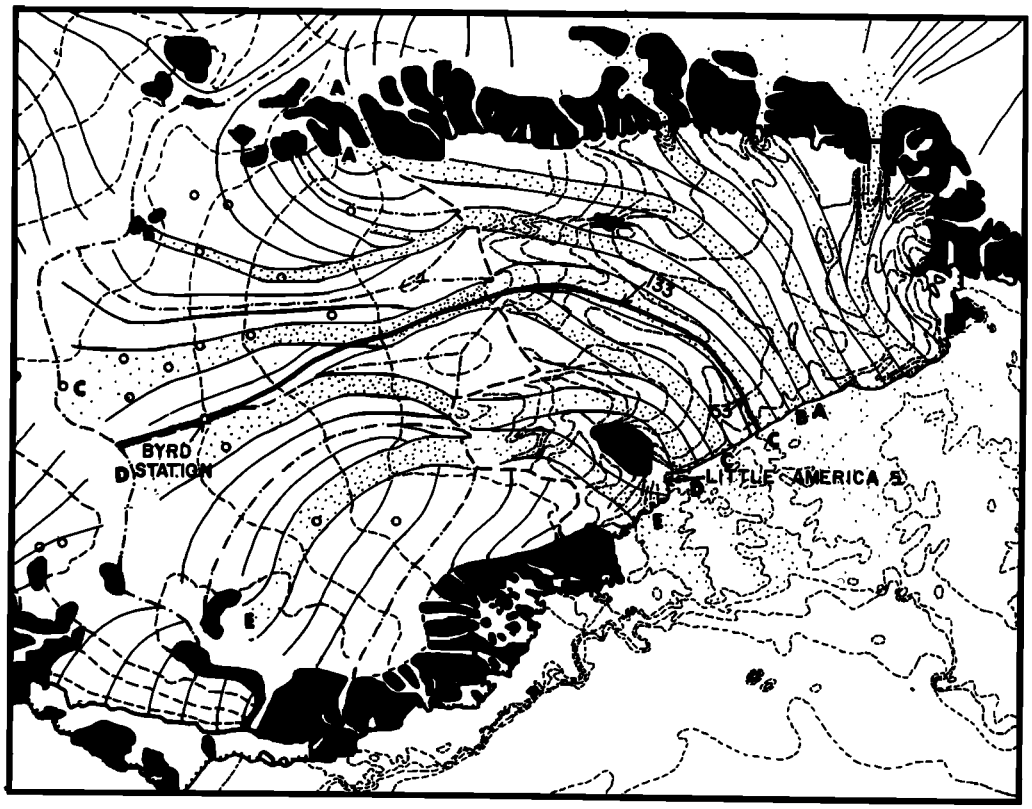

Fig. 2. Ice flowlines in the west antarctic portion of the Ross Sea ice drainage basin. Shown are (1) 500-meter ice elevation contours in Marie Byrd Land, 50-meter ice thickness contours on the Ross ice shelf, and 500-meter bathymetry contours in the Ross Sea (dashed lines), (2) ice flowlines drawn mainly normal to ice elevation and ice thickness contours (thin lines), (3) the major ice streams feeding the Ross ice shelf (dotted areas), (4) the Marie Byrd Land drainage areas of ice streams A–E (dot-dash lines), (5) areas of thick ice along Marie Byrd Land traverses (open circles), (6) mountainous regions (blackened areas), (7) ice shelf barriers (segmented lines), and (8) an ice flowline that apparently passes through Byrd Station, RISS station 133, and RISS station 53 (heavy line). (Based mainly on the SPRI-NSF radio echo flights.)

from East Antarctica and West Antarctica. The delineation of these ice streams is a result of the recent SPRI-NSF radio echo flights [*Evans and Robin*, 1972].

New information obtained from mapping ice streams, from the BSSN and RISS traverses, and from the Byrd Station and Little America 5 coreholes, make possible a stability analysis of the west antarctic portion of the Ross Sea ice drainage basin. This paper presents such an analysis.

Earlier studies of the Ross Sea ice drainage basin have usually tacitly or overtly assumed that the ice cover was stable and essentially in equilibrium, with any net positive or negative mass balance being a perturbation of a fundamentally equilibrium condition. Mass balance studies have been made for the east antarctic portion by *Giovinetto et al.* [1966], for the west antarctic portion by *Giovinetto and Zumberge* [1968], and for the Ross ice shelf by *Crary et al.* [1962*a*, 1962*b*] and *Zumberge* [1964; unpublished data, 1971]. Since the early investigators usually assume equilibrium conditions, perhaps it is not surprising that they find the ice cover to be stable or perhaps growing slightly. However, the seven remarkable features listed above suggest that the west antarctic portion may be unstable and that a prior assumption of fundamental equilibrium may be misleading. In this paper no assumption is made regarding the degree of equilibrium in the hope that the true condition of the west antarctic ice cover will then emerge.

The question of whether instability is inherent in the west antarctic ice sheet is of major importance, since its disintegration would raise sea level over 4 meters worldwide. Calculations dealing with such an important question should be supported by a full error analysis. Unfortunately, existing data make a complete error analysis impossible. For this reason, maximum error limits are employed when they are known in the hope that, when combined with terms of uncertain accuracy, an average error is obtained.

PAST AND PRESENT ICE COVER OF WEST ANTARCTICA

The glacial record in West Antarctica. Among all the drainage basins of the antarctic ice sheet, non-equilibrium concave surface profiles exist only for those parts of the west antarctic ice sheet which feed the Filchner-Ronne ice shelf between the Ellsworth Mountains and the Pensacola Mountains and feed the Ross ice shelf between the Edsel Ford Range and the Horlick Mountains. This suggests that the dynamic system of a large floating ice shelf fed by a concave ice sheet grounded below sea level represents an atypical, and hence unstable, ice cover. Instability should be reflected in the glacial record.

Figure 3 shows twenty regions preserving a record of past glaciation in Antarctica, implying an ancient ice sheet that may have extended to the continental shelf if the highest former ice levels in West Antarctica [*Wade*, 1937; *Cameron and Goldthwait*, 1961; *Craddock et al.*, 1964; *Doumani*, 1964; *Rutford et al.*, 1972; *LeMasurier*, 1972] and the Transantarctic Mountains [*Cameron and Goldthwait*, 1961; *Mercer*, 1968*a*, *b*, 1972; *Mayewski*, 1972] were contemporaneous with each other and with glacial events in the so-called 'Dry Valleys' near McMurdo Sound [*Calkin*, 1970; *Denton et al.*, 1970, 1971; *Webb*, 1972; *McSaveney and McSaveney*, 1972], on Beaufort Island [*Péwé*, 1960], on the Ross Sea floor [*Angino and Lepley*, 1966; *Houtz and Meijer*, 1970; *Chriss and Frakes*, 1972; *Fillon*, 1972], and on the Weddell Sea floor [*Anderson*, 1972]. Tracing the history of this postulated ancient ice sheet is speculative at best, and the reconstruction presented here should be compared with that by *Denton et al.* [1971]. Assuming such an ice sheet existed, dates relating to its possible history have been obtained from volcanoes along the Bakutis and Hobbs coasts of Marie Byrd Land [*LeMasurier*, 1972] and in the Jones Mountains of Ellsworth Land [*Rutford et al.*, 1972]; from lava flows, marine shells, algae, and mummified seals in the Dry Valleys region of south Victoria Land [*Nichols*, 1961; *Denton et al.*, 1970]; from oxygen isotope ratios taken from ice cores at Byrd Station [*Johnsen et al.*, 1972]; and from benthic foraminiferal faunas in the Ross Sea [*Fillon*, 1972] and the Weddell Sea [*Anderson*, 1972] that were recovered from piston cores. The history of the antarctic ice sheet postulated from this record treats only verifiable Late Cenozoic glaciations, defined as ice sheet advances strong enough to require significant advances of the Ross ice shelf and Filchner-

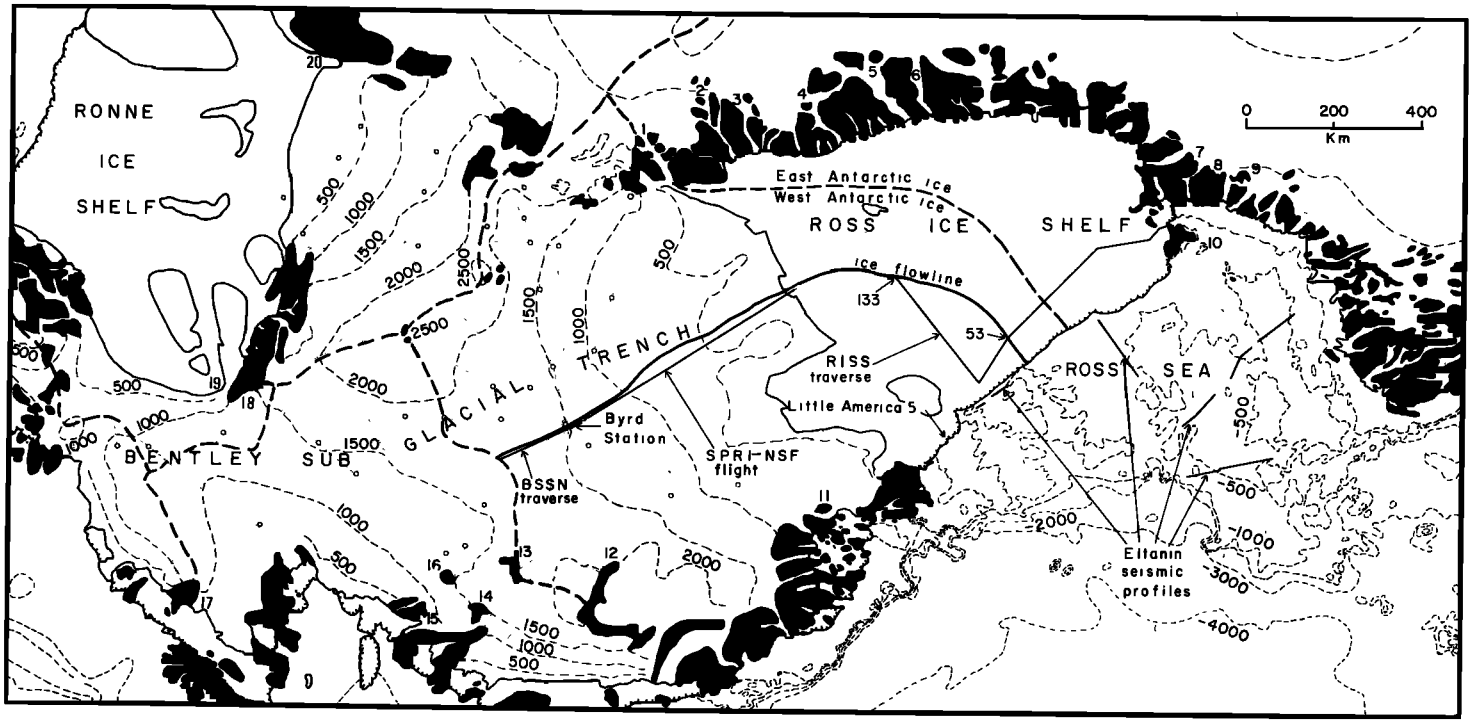

Fig. 3. Glaciological investigations in West Antarctica and adjacent parts of East Antarctica. Shown are (1) elevation contours relative to sea level, in meters (light dashed lines), (2) ice divides (heavy dashed lines), (3) traverses radiating from Byrd Station (dotted lines), (4) thick ice sites along the traverse routes (open circles), (5) the ice flowline approximately paralleling the BSSN traverse, the SPRI-NSF flight, and passing through Byrd Station, RISS station 133, and RISS station 53 (heavy line), (6) the *Eltanin* seismic profiles in the Ross Sea (straight line segments), (7) ice shelf grounding lines (solid lines) and barriers (segmented lines), and (8) twenty known regions preserving evidence of extensive past glaciation; namely, in the Transantarctic Mountains (regions 1–9), on Beaufort Island (region 10), in the Ford Ranges (region 11), inland along the Bakutis-Hobbs Coast (regions 12–16), in the Jones Mountains (region 17), in the Ellsworth Mountains (regions 18 and 19), and in the Pensacola Mountains (region 20). (Modified from *Map Sheet 13: Antarctica* [1970].)

Ronne ice shelf grounding lines. *Mercer* [1973] thoroughly reviews all available data.

Reconstructing the history of the ice cover. The postulated ancient Antarctic ice sheet would have reached the edge of the northern Marie Byrd Land continental shelf 7.0 ± 1.1 m.y. ago for the subglacial eruption of Mt. Steere (Figure 3, region 13) dated by *LeMasurier* [1972] and may have been the Taylor 5 glaciation of *Denton et al.* [1970], which covered the Dry Valleys (Figure 3, regions 7 and 8) more than 3.7 m.y. ago, since the ice sheet apparently extended to the Weddell Sea continental shelf from before 5.1 m.y. ago down to 3.3 m.y. ago [*Anderson,* 1972]. By 3.7 m.y. ago this ice sheet had retreated sufficiently to permit a marine invasion of Wright Valley (Figure 3, region 8) that brought foraminifera and pectens [*Webb,* 1972]. The retreat may also have allowed deposition of the massive till layer of the Sirius Formation [*Mercer,* 1972; *Mayewski,* 1972, 1973] in the Transantarctic Mountains (Figure 3, regions 1–9). This retreat was quite rapid, possibly the result of a surge, because the marine invasion of Wright Valley required a 600-meter depression of the valley floor, assuming no subsequent tectonic uplift [*McSaveney and McSaveney,* 1972]. Granting this, isostatic uplift could not have initially kept pace with the reduction of the ice cover. This retreat also occurred in the Weddell Sea, beginning 3.3 m.y. ago and ending perhaps 2.4 m.y. ago [*Anderson,* 1972].

A second advance of the ice sheet began between 2.7 m.y. ago and 2.1 m.y. ago in Taylor Valley, causing the Taylor 4 glaciation from the thickened plateau ice and the Ross Sea 4 glaciation from the regrounded Ross ice shelf [*Denton et al.,* 1970]. By 2.0 m.y. ago the Ross ice shelf grounding line seems to have advanced to near the continental shelf of the Ross Sea [*Fillon,* 1972], where the shallow banks described by *Angino and Lepley* [1966] are anticlines that seem to have been planed flat and sometimes deeply grooved by a sliding ice sheet [*Houtz and Meijer,* 1970]. The ice sheet remained grounded near the edge of the Marie Byrd Land continental shelf as late as 0.82 ± 0.14 m.y. ago when Mt. Murphy (Figure 3, region 15) erupted under the ice [*LeMasurier,* 1972]. This glaciation seems to have begun 2.4 m.y. ago and ended 0.3 m.y. ago in the Weddell Sea [*Anderson,* 1972]. By 0.7 m.y. ago the ice sheet had became ungrounded in the northern Ross Sea [*Fillon,* 1972], perhaps creating a floating ice shelf whose ablating underside left the drop-stone deposits described by *Chriss and Frakes* [1972]. By 0.5 ± 0.2 m.y. ago the thinning ice sheet had reached present ice elevations near Toney Mountain (Figure 3, region 14), which erupted above the ice [*LeMasurier,* 1972]. This retreat might have deposited the interbedded till and stratified lens layer covering the massive till layer of the Sirius formation in the central Transantarctic Mountains (Figure 3, regions 1–6) described by *Mercer* [1968*a*, 1972] and *Mayewski* [1972, 1973]. In the western Transantarctic Mountains (Figure 3, regions 7–9) the maximum ice elevation was below the older massive till layer deposited as the Sirius Formation by the first retreat of the ice sheet [*Mayewski,* 1972, 1973].

A third advance of the ice sheet is indicated by unusually thick ice in Marie Byrd Land where Mt. Takahe (Figure 3, region 16) erupted subglacially less than 0.24 m.y. ago [*LeMasurier,* 1972]. Ice thickening in Marie Byrd Land would have grounded the Ross ice shelf, leading to Ross Sea 3 glaciation, and ice thickening on the polar plateau of East Antarctica would have caused Taylor 3 glaciation, both in Taylor Valley [*Denton et al.,* 1970]. The corresponding glaciations in Wright Valley described by *Calkin et al.* [1970] are unresolved, owing to the new interpretation of the pecten glacial event by *McSaveney and McSaveney* [1972]. The Weddell Sea glaciation during this period began 0.255 m.y. ago and ended 0.235 m.y. ago [*Anderson,* 1972]. Retreat of the ice presumably deposited the highest lateral moraines that *Mercer* [1968*a*, 1972] found in the valleys of Reedy glacier (Figure 3, region 1) and Beardmore glacier (Figure 3, region 5). These lateral moraines are considerably lower than the basal moraines of the Sirius Formation deposited by the earlier advances.

A fourth advance of the ice sheet again grounded the Ross ice shelf, leading to the Ross Sea 2 and perhaps the loop glaciation in Taylor Valley and Wright Valley, respectively, and the concurrent ice thickening on the polar plateau led to Taylor 2 glaciation and perhaps Wright upper 4 glaciation [*Denton et al.,* 1970; *Calkin et al.,* 1970]. The Weddell Sea glaciation

during this period began 0.205 m.y. ago and ended about 0.165 m.y. ago [*Anderson*, 1972].

A fifth advance of the ice sheet more than 0.05 m.y. ago occurred when thickening ice in Marie Byrd Land again grounded the Ross ice shelf, causing Ross Sea 1 and perhaps the trilogy glaciation, and thickening ice on the east antarctic polar plateau again invaded the Dry Valleys, causing Taylor 1 and perhaps Wright upper 3 glaciation [*Denton et al.*, 1970; *Calkin et al.*, 1970]. The Weddell Sea glaciation during this period began 0.145 m.y. ago and ended 0.107 m.y. ago [*Anderson*, 1972].

The subsequent retreat may have been due to high Sangamon-Barbados interglacial temperatures and sea levels, which ungrounded the Ross ice shelf and greatly thinned the Marie Byrd Land grounded ice cover between 0.12 [*Mercer*, 1968*b*] and 0.08 m.y. ago [*Broecker et al.*, 1968; *Johnsen et al.*, 1972 corrigendum]. The retreat also thinned the ice cover on the polar plateau of East Antarctica, freeing the Dry Valleys of ice and leaving the lateral moraines above outlet glaciers through the central Transantarctic Mountains (Figure 3, regions 1–5) described by *Mercer* [1968*a*, 1972] and *Mayewski* [1972, 1973]. This deglaciation was perhaps the most extensive retreat to date for the antarctic ice sheet, since it apparently was strongly influenced by high Pleistocene interglacial temperatures and sea levels.

A minor sixth glaciation may presently be in retreat if the lowest ice-cored moraines alongside and slightly above the outlet glaciers in the central Transantarctic Mountains (Figure 3, regions 1–5) observed by *Mercer* [1968*a*, 1972] and *Mayewski* [1972, 1973] correlate with Wright upper 2 and Wright lower glaciations in Wright Valley [*Calkin et al.*, 1970]. The corresponding Weddell Sea glaciation began about 0.072 m.y. ago and ended 0.043 m.y ago [*Anderson*, 1972]. Retreat of the sixth glaciation began about 0.01 m.y. ago in the Dry Valleys [*Denton et al.*, 1970], leaving the ice-cored lateral moraine system in the outlet glacier valleys through the central Transantarctic Mountains [*Mercer*, 1968*a*, 1972; *Mayewski*, 1972, 1973] and initiating ice thinning near Byrd Station in central Marie Byrd Land 4000 years ago [*Johnsen et al.*, 1972].

Table 1 summarizes the proposed history of the west antarctic ice sheet. If this history is approximately correct, the ice sheet has been in general retreat, checked by occasional readvances, for the last few million years. Furthermore, as the ice sheet disintegrates, each recognized readvance seems to be less than the previous one and of shorter duration. However, this may be misleading because glaciations are harder to identify the older they are. Whether the ice sheet is presently advancing or retreating is considered in the following sections.

PAST AND PRESENT SURFACE PROFILES OF THE ICE SHEET

The flow law for ice in steady state creep. The external variables influencing creep are temperature T, pressure melting temperature T_M, hydrostatic pressure P, effective stress τ, effective strain ϵ, effective strain rate ϵ^*, time t, and the deformation environment. For steady state creep the effect of P can often be expressed in terms of the homologous temperature T/T_M, and the effects of ϵ and t can be expressed in terms of ϵ^*.

Nye [1953, 1957] first used τ and ϵ^* to represent the respective deviator stress components σ_{ij}' and strain rate components ϵ_{ij}^* in glaciers, where $i, j, = x, y, z$ for orthogonal axes whose origin is at the top or bottom surface of the glacier. *Glen* [1955] first showed that high temperature steady state creep in ice is thermally activated with T related to a thermal activation energy Q through the ideal gas constant R, and showed that ϵ^* increases with τ to the power n. The effect of P on the creep of ice was first studied by *Rigsby* [1958], and *Weertman* [1968] related P to T/T_M using Rigsby's data.

Many creep investigations of ice have been made, and it is now rather well established that ice obeys the flow law commonly observed for crystalline materials:

$$\epsilon^* = (\tau/A)^n = B \exp(-Q/RT)\tau^n = B \exp(-CT_M/T)\tau^n \quad (1)$$

where A, B, C, and n are parameters that in varying degrees depend on internal variables intrinsic in a particular ice specimen. These internal variables are grain configuration (size and shape), grain fabric (the pattern of optic axes), ice density (the size and concentration of trapped air bubbles), and ice purity (soluble

ions and insoluble particles). Quantitative relationships between the intrinsic variables and ice creep have generally not been experimentally determined [*Budd*, 1969; *Hughes*, 1972*c*].

Creep in the west antarctic ice sheet. Parameters C and n are most easily determined by altering the external variables of temperature and stress, respectively, and are reasonably well known. However C and n may also have separate values for basal and prismatic creep in ice [*Hughes*, 1972*c*; *Weertman*, 1972*b*]. Reasonable limits in single crystals are $C = 26 \pm 3$ and $n = 3.0 \pm 1.5$, with the lower limits for diffusion and glide in the basal planes and the upper limit for diffusion and glide in the prismatic planes [*Butkovich and Landauer*, 1958; *Itagaki*, 1964; *Higashi et al.*, 1964, 1965, 1968; *Higashi*, 1969]. For polycrystalline ice $C = 29$ is the best average, with $n = 1.5$ as a minimum value for single maximum fabrics (approximating basal glide) and $n = 3.0$ as an average value for random fabrics (mixed basal and prismatic glide). Flow law values in this paper will be based on $C = 29$ for both $n = 1.5$ and $n = 3.0$ in the hope that creep in all intermediate fabrics will be bracketed by these extreme values.

It seems likely that the variation of B with depth in the west antarctic ice cover may be relatively insensitive to location along an ice streamline. As previously mentioned, B is sensitive to the ice grain size, fabric, density, and purity. The vertical variation of these properties is remarkably similar at Byrd Station [*Gow*, 1963, 1970; *Gow et al.*, 1968] and Little America 5 [*Bender and Gow*, 1961; *Gow*, 1963, 1970; *Gow et al.*, 1968], although the former is near the Marie Byrd Land ice divide and the latter is near the Ross ice shelf barrier. Both locations are in the vicinity of a major ice stream (Figure 2). Hence the factors which control B seem to be constant along an ice stream from its origin on the grounded ice cover to its terminus on the floating ice cover, and a B value calculated at one position along the ice stream can be used at other positions. As shown by equation 1, the evaluation of B at a given position on the ice stream requires knowing the stress, strain rate, and temperature variation with depth. The vertical temperature profile at Little America 5 (Figure 5) is known from the corehole, and the simplified stress and strain rate equations for a floating ice shelf [*Weertman*, 1957] allow an average B to be calculated [*Hughes*, 1972*c*]. These values are $B = 1.9 \times 10^8$ bar^{-n} sec^{-1} for $n = 1.5$ and $B = 3.2 \times 10^9$ bar^{-n} sec^{-1} for $n = 3$, both for $C = 29$.

Past and present surface profiles of the ice cover. Toward the continental interior, former ice sheet elevations prior to the six postulated stages of retreat can be estimated from the till layers of the Sirius Formation (see appendix) and the various systems of lateral moraines in the central Transantarctic Mountains (Figure 3, regions 1–6). Toward the continental margin, former ice sheet elevations prior to the six postulated stages of retreat can be estimated from the older massive till layer of the Sirius Formation (see appendix) and the four Dry Valleys glaciation levels in the western Transantarctic Mountains (Figure 3, regions 7–9).

The twenty known regions affected by the former glaciations are located in Figure 3, and the former ice elevations in these regions are not corrected for either isostatic or tectonic changes in Table 1 (however, see appendix). It is useful to compare the present ice sheet profile along the flowline in Figure 3 with past profiles estimated from the data in Table 1. This comparison is made in Figure 4 for the oldest and youngest periods of major ice sheet advance. Along the flowline, x is horizontal and positive down the flowline, y is horizontal and normal to the flowline, z is vertical and positive upward, and the origin of the coordinates is taken at the ice-bedrock interface under the ice divide. Former ice sheet elevations along the flowline are estimated by extending y to sites in regions 1–10 in Figure 3 and using the ice elevations listed in Table 1 as the maximum ice sheet elevation along the flowline for each x, y, z coordinate. These points are the open circles in Figure 4. Since rock averages three times the density of ice, a large ice sheet (1 km or more thick) will isostatically depress the underlying bedrock an amount equal to about one-third of the ice thickness [*Weertman*, 1961]. Therefore the actual former ice elevations along the flowline in Figure 3 will be two-thirds of the distance from the present ice surface to the open circles in Figure 4, and these elevations are indicated by the solid circles.

Ice moving from the Marie Byrd Land ice

TABLE 1. Tentative Ice Sheet Elevations (in Meters) for Former

Regions	Glaciation Phase 1		Glaciation Phase 2		Glaciation Phase 3	
	Advance	Retreat	Advance	Retreat	Advance	Retreat
	7.0 ± 1.1[a]	3.5 ± 0.2	2.4 ± 0.3	0.70	0.255	0.235
	3.5 ± 0.2[b]	2.4 ± 0.3	0.82 ± 0.14	0.030	0.235	0.205
1 Reedy Glacier					2150	
1 Tillite Spur	3360[c]	3360[d]?				
2 Scott Glacier						
2 Mt. Blackburn	3440[c]					
2 Mt. Saltonstall	3500[c]					
2 Mt. Innis-Taylor	3500[c]					
3 Amundsen Glacier						
3 Mt. Wisting	3500[c]					
4 Shackleton Glacier						
4 Roberts Massif	3440[c]					
4 Mt. Block	3440[c]					
4 Dismal Buttress	3420[c]					
4 Half-Century Nunatak	3420[c]					
4 Bennett Platform	3420[c]	3420[d]				
4 Mt. Roth	3360[c]					
4 Otway Massif	3420[c]					
5 Beardmore Glacier					2100	
5 Dominion Range	3460[c]	3460[d]				
5 Mt. Deakin	3400[c]					
6 Mt. Sirius	3460[c]					
7 Mt. Feather	2800[c]					
8 Taylor Valley			1800[f]		1650[g]	
8 Wright Valley					1200[g]	
8 Shapeless Mountain	2640[c]					
9 Carapace Nunatak	2460[c]					
9 Coombs Hills	2380[c]					
9 Allan Nunatak	2320[c]					
10 Beaufort Island						
11 McKinley Peak	>770[e]					
12 Mt. Sidley	>3000					
13 Mt. Steere	3000					
14 Toney Mountain	<1600[h]					
15 Mt. Murphy	>2500[e]					
16 Mt. Takahe	>3400[e]					
17 Jones Mountains	>774					
18 Fisher Nunatak	>1792[e]					
19 Mt. Lymburner	>1940[e]					
19 Mt. Weems	>2210[e]					
20 Dufek Massif	>763[e]					

[a]Maximum age (m.y. B.P.).
[b]Minimum age (m.y. B.P.).
[c]Sirius Formation, older layer.
[d]Sirius Formation, younger layer.
[e]These peaks were covered by ice.

divide to the Ross ice shelf barrier is better approximated by parallel flowlines than by radially diverging flowlines, and for the former case the equilibrium surface profile for an ice sheet frozen to its bed is [*Haefeli*, 1961]

$$\left(\frac{h}{H}\right)^{(2n+2)/n} + \left(\frac{x}{L}\right)^{(n+1)/n} = 1 \qquad (2)$$

and for an ice sheet melted at its bed is [*Nye*, 1959]

$$\left(\frac{h}{H}\right)^{(2n+4)/(n+1)} + \left(\frac{x}{L}\right)^{(n+3)/(n+1)} = 1 \qquad (3)$$

where h and x are vertical height and horizontal length, respectively, measured from the base of an ice sheet at the ice divide, H and L are their maximum values, the bottom of the ice

Antarctic Glaciations Related to the 20 Regions in Figure 3

Glaciation Phase 4		Glaciation Phase 5		Glaciation Phase 6		
Advance	Retreat	Advance	Retreat	Advance	Retreat	
0.205	0.165	0.145	0.107	0.072	0.043	
0.165	0.145	0.107	0.072	0.043	0	References
1800		1660		1400		*Mercer* [1968*a*, 1972]
				1800		*Mercer* [1968*a*, 1972]
1300		1120		910		*Mayewski* [1972]
				2400		*Mayewski* [1972]
				2400		*Mayewski* [1972]
				2400		*Mayewski* [1972]
1600		1300		1200		*Mayewski* [1972]
				2000		*Mayewski* [1972]
1840		1630		1400		*Mayewski* [1972]
				2200		*Mayewski* [1972]
				2600		*Mayewski* [1972]
				2300		*Mayewski* [1972]
				2600		*Mayewski* [1972]
				1700		*Mayewski* [1972]
				300		*Mayewski* [1972]
				2200		*Mayewski* [1972]
1960		1300		750		*Mercer* [1968*a*, 1972]
				1800		*Mayewski* [1972]
				1200		*Mayewski* [1972]
				1900		*Mercer* [1968*a*, 1972]
				2000		*Mayewski* [1972]
1450[h]		650[i]		0		*Denton et al.* [1970]
1000[h]		800[i]		0		*Calkin et al.* [1970]
				2400		*Mayewski* [1972]
				2000		*Mayewski* [1972]
				2000		*Mayewski* [1972]
				2000		*Mayewski* [1972]
		200		0		*Péwé* [1960]
				750		*Wade* [1937]
				2550		*Doumani* [1964]
				1500		*LeMasurier* [1972]
				1600		*LeMasurier* [1972]
				500		*LeMasurier* [1972]
				1300		*LeMasurier* [1972]
				558		*Rutford et al.* [1972]
				1610		*Cameron and Goldthwait* [1961]
				1600		*Craddock et al.* [1964]
				1600		*Craddock et al.* [1964]
				523		*Cameron and Goldthwait* [1961]

[f] Taylor 4 and Ross 4 glaciations.
[g] Taylor 3 and Ross 3 glaciations.
[h] Taylor 2 and Ross 2 glaciations; Wright Upper 4 and Loop glaciations.
[i] Taylor 1 and Ross 1 glaciations; Wright Upper 3 and Triology glaciations.

sheet is flat, the top of the ice sheet has constant accumulation, and an average value of A can be used in the flow law (1). The bottom of the west antarctic ice sheet is not flat but averages about 500 meters below sea level. This elevation is a surface of constant τ_{zz} in the ice and is the effective bed of the ice sheet when applying (2) and (3) [*Weertman*, 1961; *Budd*, 1970]. The top of the ice sheet has a rather uniform snow accumulation in Marie Byrd Land and on the Ross ice shelf [*Bull*, 1971], and in any case moderate variations in snow accumulation will not significantly alter the ice sheet profile [*Nye*, 1959]. From the observed general correspondence of the profiles of temperature and ice physical properties down the coreholes at Byrd Station and Little America 5. it is possible to use an average A in (1). The shape of the surface profiles predicted by (2) and (3) must be modified somewhat at the center

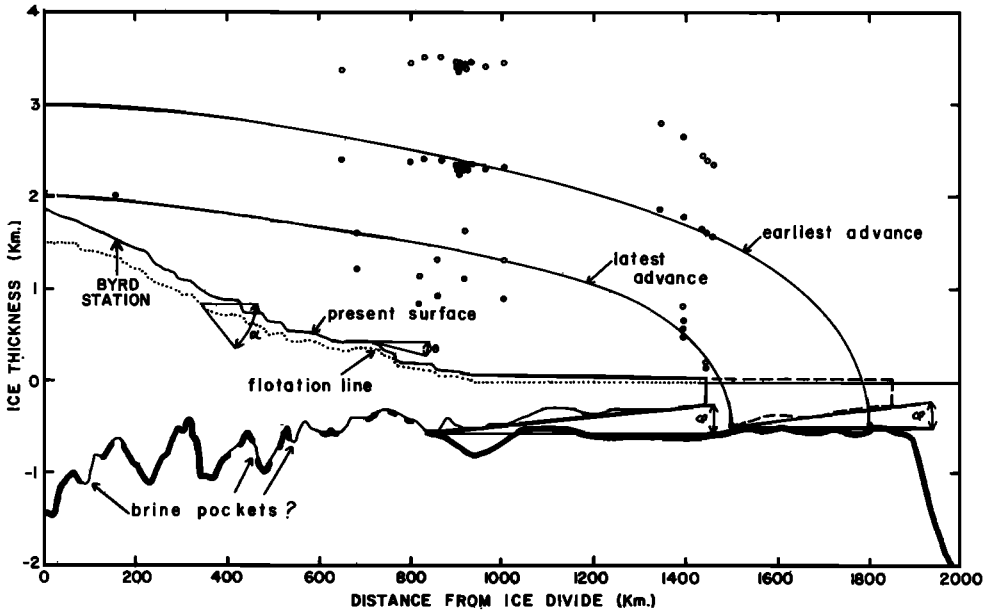

Fig. 4. Past and present profiles along the ice flowline shown in Figures 2 and 5. Shown are (1) present elevations of bedrock (heavy line), the flotation buoyancy line (dotted line), and the ice sheet top surface (light line), (2) regions of strong seismic sounding and radio-echo basal reflections, possibly brine pockets trapped when the ice cover became grounded, (3) the angle of present ice top surface slope θ, the angle of flotation line slope α, and the gross angle between bedrock and the bottom ice shelf surface φ, (4) estimated past ice elevations with (solid circles) and without (open circles) reductions for isostatic depressions, and (5) theoretical wet-base equilibrium surface profiles for the oldest and youngest known glacial advances, (6) elliptic quadrants and (7) probable ice shelf during youngest known glacial advance (dashed line). (From the SPRI-NSF flights, appendix, and data by *Mayewski* [1972].)

[*Weertman*, 1961] and the edge [*Nye*, 1967] of the ice sheet, but these adjustments are not necessary for the purpose of this paper.

The thin line segments along the bed in Figure 4 locate regions along the flowline in Figure 3, where basal melting has been detected by seismic sounding [*Dewart*, 1973], by coring [*Gow et al.*, 1968], and by radio echo sounding [*Robin et al.*, 1970*b*]. Basal melting under the the entire Marie Byrd Land ice cover is predicted theoretically [*Zotikov*, 1963; *Budd et al.*, 1970]. Therefore (3) is used as a theoretical fit to the estimated former ice elevations in Figure 3, where $n = 3$ gives the best fit (this is why $n = 3$ was used in the appendix). Apparently the west antarctic ice cover was an equilibrium ice sheet during these former glaciations, since (2) and (3) give equilibrium surface profiles. It is obvious that the present surface profile cannot be matched to either of these equations for any n, strongly indicating that the present west antarctic ice cover is a nonequilibrium ice sheet.

Dating the latest instability in the former ice cover. The former ice elevations indicated in Figure 6 are supported by the profile of the oxygen isotope ratio $\delta = {}^{18}O/{}^{16}O$ down the coreholes at Byrd Station [*Johnsen et al.*, 1972] and Little America 5 (Dansgaard, personal communication, 1972). Using the oxygen isotope profile down the corehole at Camp Century, Greenland, as a standard (because the entire Camp Century record shows excellent correlation with climatic events known from independent sources) Johnsen et al. believe that the west antarctic ice sheet has undergone considerable fluctuations during the last 80–100 millenia. Since δ increases about 1‰ per degree Centigrade, and the adiabatic lapse rate is about 1°C increase per 100-meter decrease in elevation, an increase of δ with time can be interpreted as an increasing deposition tempera-

ture due to climatic warming over the ice sheet, reduction in elevation of the ice sheet, or both. If climate has been stable, Johnsen et al. show from the δ profile at Byrd Station that some 80,000 years ago the west antarctic ice cover was nearly 1000 meters lower than at present and coincided with the Barbados 1 high sea level [*Broecker*, 1968]. The general climatic trend during the last 8000 years is in phase for both hemispheres [*Auer*, 1960] and comparing the Byrd Station and Camp Century δ profiles over this period leads Johnsen et al. to conclude that beginning 4000 years ago the mass balance of the west antarctic ice sheet turned strongly negative and led to a reduction in ice thickness of 300–500 meters at Byrd Station (in their definition, a negative mass balance occurs when snowfall is insufficient to maintain an ice elevation that is being lowered by downstream flow).

When the mass balance turned negative, presumably nonequilibrium conditions initiated the instability zone that now separates the concave and convex portions of the grounded ice cover. Along this zone, $d^2h/dx^2 = 0$, and if this zone is presently moving inland, the reduction in ice elevation was first experienced at the grounding line. According to data plotted in Figure 4, the most recent equilibrium ice sheet was grounded near the present barrier of the Ross ice shelf using the grounding line proposed by *Houtz and Meijer* [1970]. From the glacial geology in south Victoria Land, *Denton et al.* [1970] find that the latest Ross Sea glaciation began its retreat not later than 9500 years ago. This retreat was not experienced upstream from Byrd Station until about 4000 years ago according to the oxygen isotope data, and by this time glacial geology studies in south Victoria Land show that the open sea had reached the former grounding line near the present ice barrier [*Denton et al.*, 1970] and isostatic uplift had begun [*Nichols*, 1961].

The difference between the youngest (lowest) ancient ice profile and the present ice profile in Figure 4 represents an ice loss of about 1.5×10^6 km^3 for the west antarctic portion of the Ross Sea ice drainage basin. This volume of ice would result in a sea level increase averaging 0.75 ± 0.15 mm yr^{-1} over the last 4000–6000 years and compares with independent estimates of the rate of increase during this period [*Shepard*, 1963; *Jelgersma*, 1966; *Redfield*, 1967; *Scholl and Stuiver*, 1967; *Scholl et al.*, 1969].

The isostatic response to a reduction of the ice cover. If the former west antarctic ice cover was as thick as indicated in Figure 4, the underlying bedrock must have been isostatically depressed [*Weertman*, 1961]. Negative free air gravity anomalies predominate over both Marie Byrd Land [*Robinson*, 1964; *Bentley and Chang*, 1971] and the Ross ice shelf [*Bennett*, 1964]. However, less accurate Marie Byrd Land surface elevations place the negative anomalies within the errors of measurement. With the present elevation uncertainties in Marie Byrd Land, ice thickness reductions of several hundred meters would be undetected by gravity measurements [*Bentley*, 1964]. Over the Ross ice shelf, however, isostatic uplift can be detected, and *Bennett* [1964] calculates that 600 meters of sediment would have accumulated under the Ross ice shelf if it became ungrounded 10,000 years ago. Hence the isostatic uplift adjustment in Figure 4 should probably not be made for the most recent glacial advance, and the equilibrium surface profile over the Ross ice shelf does fit the open circles better than the solid circles.

THE GROUNDED ICE COVER

Instability and the surface profile. Equilibrium surface profiles are calculated from τ_{xz}, which is responsible for the laminar flow component of a grounded ice sheet. When basal sliding does not occur the effect of τ_{xz} is distributed throughout the ice and (2) gives the surface profile [*Haefeli*, 1961], but when basal sliding occurs the effect of τ_{xz} becomes largely concentrated at the bed and (3) gives the surface profile [*Nye*, 1959]. Disregarding local variations related to bed topography and meteorological effects, the west antarctic ice sheet surface is convex only near the ice divide, and becomes concave toward both the Ronne ice shelf and the Ross ice shelf (Figure 3). As (2) and (3) show, an equilibrium surface profile must be convex, and, according to Figure 4, the west antarctic grounded ice cover did have a convex surface in the past. Therefore one might ask if the surface profile inflection point near Byrd Station is migrating inland. If so, the west antarctic ice cover is still disintegrating.

Instability and ice velocity. The present

stability of the grounded portion of the west antarctic ice cover can be addressed by considering the results of the BSSN traverse [*Dewart*, 1973; *Brecher*, 1973; *Whillans*, 1973*a*, *b*]. The BSSN traverse parallels the broad trend of the ice streamlines that pass through Byrd Station, and only a slight divergence of these streamlines is observed [*Whillans*, 1973*a*, *b*], so that lateral flow will be relatively insignificant compared to downstream flow.

The stress and strain rate vertical profiles through a grounded ice sheet unable to slip on its bed are those for the lower half of a viscoplastic material compressed between inclined, frictional, parallel plates [*Nye*, 1957]. Take x as horizontal and positive downstream, y as horizontal and normal to the flow direction, z as vertical and positive upward, and the origin of these orthogonal coordinates to be at the base of the ice sheet. For no flow in the y direction and no slip along the bed

$$\sigma_x = \sigma_z \pm 2(\tau^2 - \tau_{xz}^2)^{1/2} \tag{4a}$$

$$\sigma_z = \rho g(h - z) \cot \theta \tag{4b}$$

$$\tau_{xz} = \rho g(h - z) \tan \theta \tag{4c}$$

where θ is the angular inclination. For ice sheets, θ is the top surface slope.

The BSSN consists of two parallel lines of posts, posts 1–103 are odd, and posts 2–104 are even. Surface strains were measured for the 51 quadrilaterals defined by four posts each. Let u, v, and w be the respective velocity components along x, y, and z, with single-prime and double-prime terms applying to upstream and downstream points, respectively, along a flowline. For a BSSN quadrilateral, single-prime terms apply to the upstream pair of posts and double-prime terms apply to the downstream pair of posts. Hence, longitudinal horizontal distances from the ice divide are x' and x'', lateral horizontal distances between post pairs are $\Delta y'$ and $\Delta y''$, mean vertical ice thicknesses for each post pair are h' and h'', horizontal longitudinal ice velocities are u' and u'', and the net ice accumulation rate within the quadrilateral is a. For each quadrilateral, $\Delta x = x'' - x'$, $\Delta y = \Delta y'' - \Delta y'$, $\Delta h = h'' - h'$, $\Delta u = u'' - u'$, and $a = a_t + a_b$, where a_t and a_b are the top surface and bottom surface net ice accumulation rates, respectively. The longitudinal, lateral, and vertical strains are $\epsilon_x = (x'' - x')/x'$, $\epsilon_y = (\Delta y'' - \Delta y')/\Delta y'$, and $\epsilon_z = (h'' - h')/h'$, respectively. Average values are $\langle x \rangle$, $\Delta\langle y \rangle$, $\langle h \rangle$, and $\langle u \rangle$.

Applying the temperature profile at Byrd Station to the BSSN, the curve in Figure 5 being approximated by two straight lines, for $0 \leq z/h \leq \frac{1}{2}$,

$$\frac{T_M}{T} \cong 1 + \frac{\Delta[(T_M/T) - 1]}{\Delta(z/h)} \left(\frac{z}{h}\right) = 1 + \beta(z/h) \tag{5}$$

and for $\frac{1}{2} \leq z/h \leq 1$,

$$T_M/T \cong \beta' \tag{6}$$

where $\beta = 0.24$ and $\beta' = 1.114$ are for the linear approximations.

Posts 1–2 at the downstream BSSN terminus are close to Byrd Station, and both snow accumulation and surface velocity at these posts seem to be affected by the presence of Byrd Station (Figure 6). Hence posts 3–4 will be used in the following calculations because they seem to be more typical of the downstream end of the BSSN. Let u_t be the measured top surface velocity at BSSN posts 3–4. Assuming zero velocity at the ice divide, u_t is the summation over $j = 51$ quadrilaterals of the top surface velocities Δu_t inside quadrilaterals. Using (1),

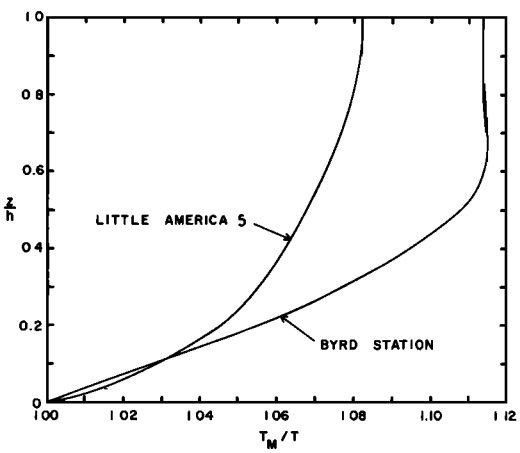

Fig. 5. Reciprocal homologous temperature T_M/T versus normalized ice thickness z/h down the Little America 5 and Byrd Station coreholes. (From *Bender and Gow* [1961] and *Gow et al.* [1968].)

(5), and (6), where u_b is the basal sliding velocity and u_c is the differential shear creep velocity,

$$
\begin{aligned}
u_t &= \sum_i \Delta u_t = u_b + u_c \\
&= \int_0^z \epsilon_b^* \, dx + \int_0^h \gamma_c^* \, dz \\
&= u_b + \int_0^h 2A^{-n}\tau^{n-1}\tau_{xz} \, dz \\
&= u_b + \int_0^h \frac{2}{A^n} \\
&\quad \cdot \left[\left(\frac{\sigma_x - \sigma_z}{2}\right)^2 + \tau_{xz}^2\right]^{(n-1)/2} \tau_{xz} \, dz \\
&= u_b + \int_0^h \frac{2}{A^n}\left(\frac{\epsilon_x^{*2} + \epsilon_{xz}^{*2}}{\epsilon_{xz}^{*2}}\right)^{(n-1)/2} \tau_{xz}^n \, dz \\
&\cong u_b + \int_0^h 2A^{-n}\tau_{xz}^n \, dz \\
&= u_b + 2(\rho g \tan\theta)^n \int_0^h A^{-n}(h-z)^n \, dz \\
&\cong u_b + 2(\rho g \tan\theta)^n B \\
&\quad \cdot \left[\int_0^{h/2} \exp\left[-C(1+\beta(z/h)\right](h-z)^n \, dz \right. \\
&\quad \left. + \int_{h/2}^h \exp\left(-C\beta'\right)(h-z)^n \, dz\right] \\
&\cong u_b + B(\rho g \tan\theta)^n h \exp(-C) \\
&\quad \cdot \left[\frac{\exp\left[-C(\beta'-1)\right]}{2^n(n+1)} \right. \\
&\quad \left. + 2\sum_{i=1}^{i=m}(-1)^{i+1}\frac{m^{i+1}}{(C\beta)^i}\right] \qquad (7)
\end{aligned}
$$

Here $\gamma_c^* = 2\epsilon_c^*$ is the differential shear creep strain rate and becomes a laminar flow strain rate when $\epsilon_z^* = 0$ so that $\epsilon_c^* = \epsilon_{xz}^*$. *Nye* [1959] demonstrated convincingly that this simplification is justified by analyzing flow at station A125 (78°N, 53°W) on the British North Greenland Expedition traverse, where h, θ, and T were comparable to the BSSN values. Along the downstream portion of the BSSN average values are $h = 2500$ meters and $\tan\theta = 2 \times 10^{-3}$, giving $u_c = 3.22$ m yr^{-1} for $n = 1.5$ and $u_c = 1.65$ m yr^{-1} for $n = 3.0$, using the previously specified values of ρ, g, B, C, β, and β'. Both values of n are included by taking $u_c = 2.5 \pm 1.0$ m yr^{-1}. Figure 6 gives $u_t = 11.0$ m yr^{-1} at BSSN posts 3–4. Therefore, $u_b = 8.5 \mp 1.0$ m yr^{-1} from (7), where $m = 5$ suffices.

Let $\langle u \rangle_c$ be the differential shear creep velocity averaged through h, then

$$
\begin{aligned}
\langle u \rangle_c &= \frac{1}{h}\int_0^h u_c \, dz = \frac{1}{h}\int_0^h \int_0^z \gamma_c^* \, dz \, dz \\
&= (2/h)(\rho g \tan\theta)^n \\
&\quad \cdot \int_0^h \int_0^z A^{-n}(h-z)^n \, dz \, dz \qquad (8)
\end{aligned}
$$

Equation 8 can be graphically integrated or solved by using the method of successive approximations described by *Nye* [1959]. The result is $\langle u \rangle_c = 2.0 \pm 1.0$ m yr^{-1}, which includes values for both $n = 1.5$ and $n = 3.0$.

The mass balance for a BSSN quadrilateral is obtained from conservation of volume and is illustrated in Figure 6:

$$
\begin{aligned}
\Delta y'' h'' u'' &= \Delta y' h' u' \\
&\quad + \tfrac{1}{2}(\Delta y'' + \Delta y')(x'' - x')a \qquad (9a)
\end{aligned}
$$

$$
\begin{aligned}
a &= \frac{h'u'\epsilon_y + h'\,\Delta u(1+\epsilon_y)}{\Delta x(1+\epsilon_y/2)} \\
&\quad + \frac{u'\,\Delta h(1+\epsilon_y) + \Delta h\,\Delta u(1+\epsilon_y)}{\Delta x(1+\epsilon_y/2)} \qquad (9b)
\end{aligned}
$$

Let u_m be the mass balance velocity summed over j quadrilaterals. Therefore

$$
\begin{aligned}
u_m &= \sum_j \left[\left(\frac{\Delta y' h'}{\Delta y'' h''}\right)u' \right. \\
&\quad \left. + \left(\frac{(\Delta y'' + \Delta y')(x'' - x')}{2\,\Delta y'' h''}\right)a\right] \\
&= \sum_j \left[\frac{u'}{(1+\epsilon_y)(1+\epsilon_z)} + \frac{(2+\epsilon_y)\,\Delta x a}{2(1+\epsilon_y)h''}\right] \\
&\cong \sum_j \left[\frac{u'}{(1-\epsilon_z)} + \frac{(2+\epsilon_y)\,\Delta x(a_t + a_b)}{2(1+\epsilon_y)h''}\right] \\
&\qquad (10)
\end{aligned}
$$

where $(1+\epsilon_y)(1+\epsilon_z) \cong 1 + \epsilon_y + \epsilon_z = 1 - \epsilon_x$, since $\epsilon_x + \epsilon_y + \epsilon_z = 0$ by conservation of volume. Equation 10 is plotted in Figure 6 for a_t only, giving $(u_m)_t = 9.0$ m yr^{-1} at BSSN posts 3–4 due to snow accumulation on the top surface. Note that $u_m = u''$ when $j = 1$, as is required by (9a).

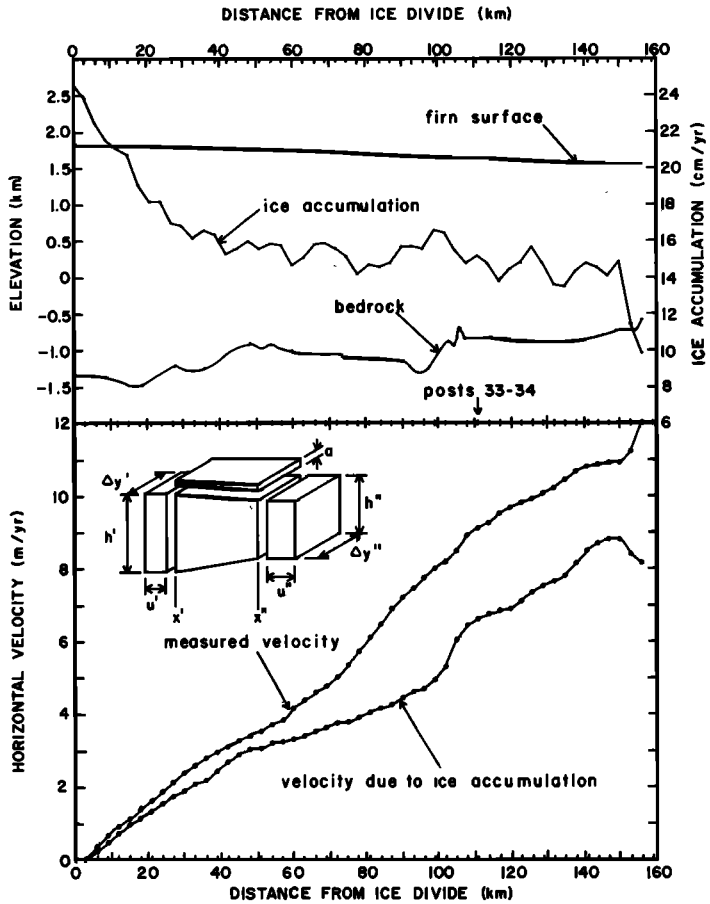

Fig. 6. Glaciological results along the 51 west slope quadrilaterals of the BSSN. Shown are (1) firn and bedrock elevations, (2) snow accumulation in ice equivalent, (3) surface ice velocity measured from the strain network, (4) the component of surface ice velocity due to ice accumulation, corrected for lateral and vertical convergence or divergence, (5) a diagram showing how the mass flux through a strain net quadrilateral was calculated, and (6) posts 33–34 where a reversed phase seismic reflection preceded the main reflection. (Based on data by *Dewart* [1973], *Brecher* [1973], and *Whillans* [1973*a*, *b*].)

When the ice sheet is in equilibrium, the mass balance velocity u_m will equal the steady state velocity u_s, where $u_s = u_b + \langle u \rangle_c$. Under non-equilibrium conditions there will be a net velocity increment δu due to mass imbalance, where

$$\delta u = u_m - u_s$$

$$= [(u_m)_i + (u_m)_b] - [u_b + \langle u \rangle_c] \qquad (11)$$

Zotikov [1963] and *Budd et al.* [1970] have determined from theoretical considerations that the central portion of West Antarctica is a region of basal ablation. Hence $a_b < 0$ is expected along the BSSN, so that $(u_m)_b < 0$ at post 3–4. Solving (11) using $(u_m)_i = 9.0$ m yr^{-1}, $u_b = 8.5 \mp 1.0$ m yr^{-1}, and $\langle u \rangle_c = 2.0 \pm 1.0$ m yr^{-1} from the analysis of BSSN data, gives $\delta u = -1.5$ m yr^{-1} at BSSN posts 3–4 even without basal melting. Ice is moving downstream faster than it is being replaced by snowfall upstream, and the BSSN has a negative mass balance of at least 17%.

Errors associated with the choice of n in the flow law tend to cancel in computing u_s, and the temperature profile insures a small error in u_s, even in the extreme case of perfectly plastic flow versus perfectly viscous flow. Uncertainties in snow accumulation and surface strain as

reported by *Brecher* [1973] and *Whillans* [1973*a*, *b*] are under 10% of measured values. Therefore the conclusion that mass balance is negative along the BSSN seems reasonable, provided present snow accumulation rates were not significantly greater in the past few millenia. Furthermore, this conclusion has independent support from the analysis of oxygen isotope ratios for the Byrd Station corehole, as reported by *Johnsen et al.* [1972].

Instability and ice streams. Downstream from Byrd Station the general trend is a decrease of both θ and h with distance from the ice divide, although great local variations occur (Figure 4). *Zotikov* [1963] and *Budd et al.* [1970] predict a sign reversal of a_b toward the Ross ice shelf grounding line, with increasing basal freezing rates downstream from Byrd Station. A progressive decrease of θ and h in (7) combined with an increasingly positive a_b in (10) tend to restore equilibrium conditions since $u_s \rightarrow u_m$ in (11). If flow tends to concentrate in ice streams, however, frictional heat will increase in the downstream direction as the ice streams accelerate. Hence a_b might become increasingly negative in ice streams and tend to preserve local nonequilibrium flow by neutralizing the effects of decreasing θ and h.

Ice drainage from Marie Byrd Land into the Ross Sea seems to be mainly channeled into the large ice streams shown in Figure 2. Each ice stream has its own drainage area in the Ross Sea ice drainage basin, and Figure 7 shows these drainage areas and the snow accumulation (ice equivalent) in each area. The width and depth of the ice streams near the grounding line have been determined by *Robin et al.* [1970], and with the snow accumulation data for Marie Byrd Land [*Bull*, 1971] an estimate of the mass balance ice velocity in and between ice streams can be made along the Ross ice shelf grounding line. Table 2 presents the results, namely that 86% of the Marie Byrd Land annual ice input is discharged by ice streams B, C, D, and E and that ice crossing the grounding line averages 470 m yr^{-1} in the ice streams and only 50 m yr^{-1} between ice streams. Therefore these ice streams control the rate of ice discharge from the grounded ice cover, and any instability which initiated a surge would presumably have its most dramatic effects in the ice streams. In fact, relative to the ice cover between them, the ice streams are permanently surging because they attract basal meltwater [*Weertman*, 1969, 1972*a*]. In Table 2, $a_b = 0$ is assumed.

THE FLOATING ICE COVER

The flow regime of the Ross ice shelf. The flowline shown in Figure 2 is of interest not only because past and present ice profiles can be constructed along it but also because absolute velocities along it are known for the portion along the BSSN (assuming absolute velocity is zero at the ice divide) and at RISS stations 133 and 53. Table 3 lists the ice velocity, ice thickness, and flowline length at the ice divide, BSSN posts 3–4, RISS station 133, and RISS station 53. In general, there is a net convergence of flowlines from the ice divide to the ice barrier, but the major ice streams experience divergent flow immediately downstream from the grounding line and around local grounding points that appear as islands or ice rises on the ice shelf (Figures 2 and 8).

Flowlines on the Ross ice shelf can be approximately traced by relating ice thickness contours to the major ice streams along the grounding line and to the absolute ice velocities along the N-S and E-W legs of the RISS traverse. This has been done in Figure 8. Note that the major ice streams feeding the ice shelf remain defined by the ice thickness contours but are practically unrecognizable from the absolute velocity vectors. The grounding line ice input rates for the major ice streams of West Antarctica and East Antarctica are given in Table 2 and Figure 9, respectively. Comparing these input rates with the RISS absolute velocity vectors in Figure 9 emphasizes the capacity of the floating ice cover to dampen ice stream flow. The fact that floating ice streams tend to merge velocities while retaining individual topographic identity might be explained by a surge. Ice elevation in a surging glacier is decreased in the upstream collapsed portion and increased in the downstream advancing portion, causing a concave upstream profile and a convex downstream profile. Ice streams on the Marie Byrd Land side of the Siple Coast grounding line have a lower elevation than the flanking ice and their continuations on the Ross ice shelf side of the Siple Coast grounding line have a higher elevation than the flanking ice. Therefore, perhaps the west antarctic ice sheet has

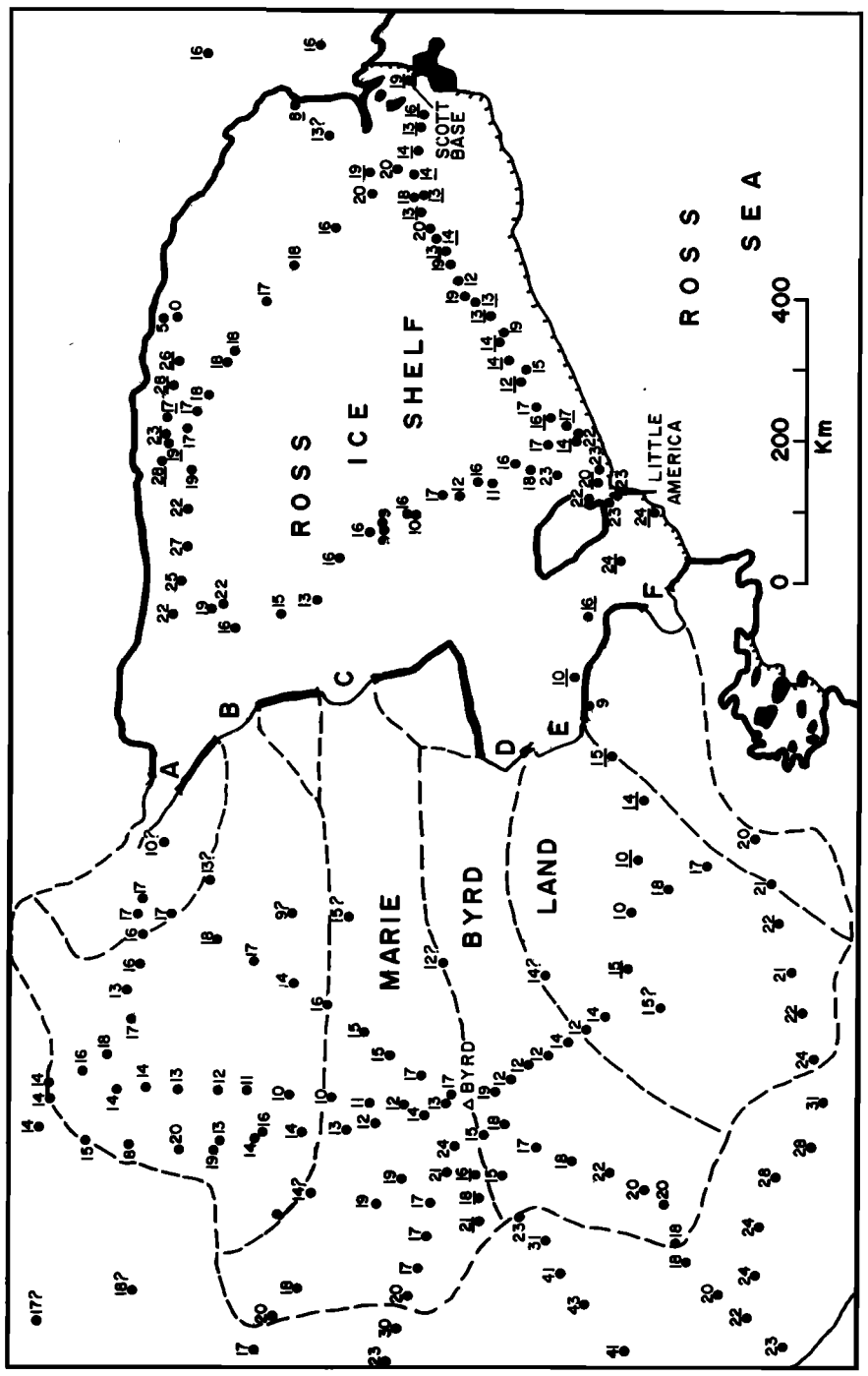

Fig. 7. Snow accumulation over Marie Byrd Land and the Ross ice shelf. Shown are (1) locations and amounts (in gm cm^{-2} yr^{-1}) of snowfall (solid numbered circles with most accurate numbers underlined), and (2) ice drainage regions for and between the major ice streams A–F in Marie Byrd Land (dashed lines, see also Figure 2). (Modified from *Bull* [1971].)

TABLE 2. Accumulation in the Ross Sea Ice Drainage Basin of Marie Byrd Land and Discharge along the Siple Coast Assuming Equilibrium and Zero Basal Balance

Region (Figure 7)	Marie Byrd Land Area, km^2	Accumulation,[a] gm cm^{-2} yr^{-1}	Volume, km^3 yr^{-1}	Siple Coast Width,[b] km	Thickness,[b] meters	Velocity, m yr^{-1}
A[c]				45	1000	
AB[d]	27,500	15.0	4.50	90	700	71
B	175,500	15.0	28.63	75	800	477
BC	8,750	15 ?	1.43	85	750	22
C	165,800	16.1	29.50	85	660	526
CD	14,500	15 ?	2.37	120	830	24
D	126,200	16.3	22.45	60	850	440
DE				15		
E	152,000	16.5	27.38	80	800	428
EF	49,500	16.8	9.07	200	550	82
F				40	350	

[a] *Bull* [1971].
[b] *Robin et al.* [1970].
[c] Drainage regions of major ice streams.
[d] Drainage regions between major ice streams.

surged, with the Marie Byrd Land portion being the concave zone of collapse and the Ross ice shelf portion being a remnant of the downstream zone of advance. Such a rapid advance would explain why the major ice streams preserved their topographic definition but lost their velocity definition when they became ungrounded. Former grounding lines in the northern Ross Sea would allow the presurge ice streams to erode the sea floor, and the elongated sea floor troughs shown in Figures 2 and 3 can be approximately matched with the ice thickness imprint of ice streams on the Ross ice shelf shown in Figures 2 and 8.

Ice streams A and C are identified in Figure 2, and Figure 9 shows their central flowlines in relation to absolute ice velocity vectors along the RISS traverse, where ice stream A separates east antarctic ice from west antarctic ice and ice stream C passes through RISS stations 133 and 53. It seems clear that ice leaving the Siple Coast of West Antarctica flows around Roosevelt Island to the Ross ice shelf barrier. The longitudinal strain rate ϵ_x* is positive since absolute velocity vectors on the RISS E-W leg exceed those on the RISS N-S leg. The lateral strain rate ϵ_y* is negative since ice streams A through D converge (Figure 2). The simple shear strain rate γ_{yx}* is positive because absolute velocity vectors on the RISS N-S and E-W legs are relatively constant (in fact, velocity even tends to decrease toward the southern end of the RISS N-S leg).

TABLE 3. Data along the Flowline in Figure 3

	u, m yr^{-1}	h, meters	x, km
Ice Divide	0	3150[c]	0
BSSN Posts 3-4	12 ± 1[a]	2280[c]	153
Grounding Line		660[d]	780
RISS Station 133	323 ± 4[b]	480[b]	1065
RISS Station 53	841 ± 5[b]	350[b]	1365

[a] *Whillans* [1973a, b].
[b] *Dorrer et al.* [1969], *Dorrer* [1970].
[c] *Dewart* [1973].
[d] *Robin et al.* [1970].

Basal melting along the Siple Coast grounding line. Basal freezing over large areas of the Ross ice shelf is not expected from a consideration of steady state heat flow [*Robin*, 1968], radio echo results [*Robin et al.*, 1970*b*], or mass balance calculations for Antarctic ice shelves in general [*Thomas and Coslett*, 1970]. However, Ross Sea salinity increases as the Ross ice shelf barrier is approached from the north [*Jacobs et al.*, 1970], and this could be caused by salt being expelled at the sea-ice interface under the Ross ice shelf if the net basal freezing predicted by *Zumberge* [1964] occurs.

Even if net basal freezing occurs under the Ross ice shelf, Figure 10 shows that basal melting increases rapidly toward the ice barrier [J. H. Zumberge, unpublished data, 1971], and

it can rather convincingly be shown that a similar increase toward the grounding line is likely. From Table 2, the average Siple Coast grounding line · mass balance ice velocity is about 260 m yr^{-1} and is about 526 m yr^{-1} for ice stream C which passes through RISS station 133. From Table 3, the absolute ice velocity is 323 ± 4 m yr^{-1} at RISS station 133, and this velocity includes a longitudinal ice shelf spreading rate of several hundred meters per year [*Hughes*, 1972*c*] if no net basal melting occurs along ice stream C between the Siple Coast and RISS station 133. Therefore, basal melting is highly likely in this region and is probably concentrated along the grounding line because the ice shelf seems to thin dramatically in this region [*Thiel and Ostenso*, 1961].

Retreat of the Ross ice shelf grounding line. High ablation rates along the grounding line should cause grounding line recession. If the Ross ice shelf grounding line began retreating 10,000 years ago from a position about 80 km north of the present ice barrier, as has been suggested, the average retreat rate has been about 70 m yr^{-1}. During this time, sea level has apparently increased an average of about 1 mm yr^{-1} [*Shepard*, 1963; *Jelgersma*, 1966; *Redfield*, 1967; *Scholl and Stuiver*, 1967; *Scholl et al.*, 1969]. Referring to Figure 4, for the flowline under consideration the length of the floating ice shelf is about 600 km and the basal ice is about 300 meters above the sea floor at the ice barrier. This gives $\varphi \cong 5 \times 10^{-4}$, where φ is the gross angle between the ice shelf base and the sea floor at the grounding line; φ is not greatly changed for the former ice shelf profile proposed in Figure 4. Keeping φ constant during a sea level increase of 1 mm yr^{-1} requires the grounding line to retreat an average of 2 m yr^{-1} over the past 10,000 years.

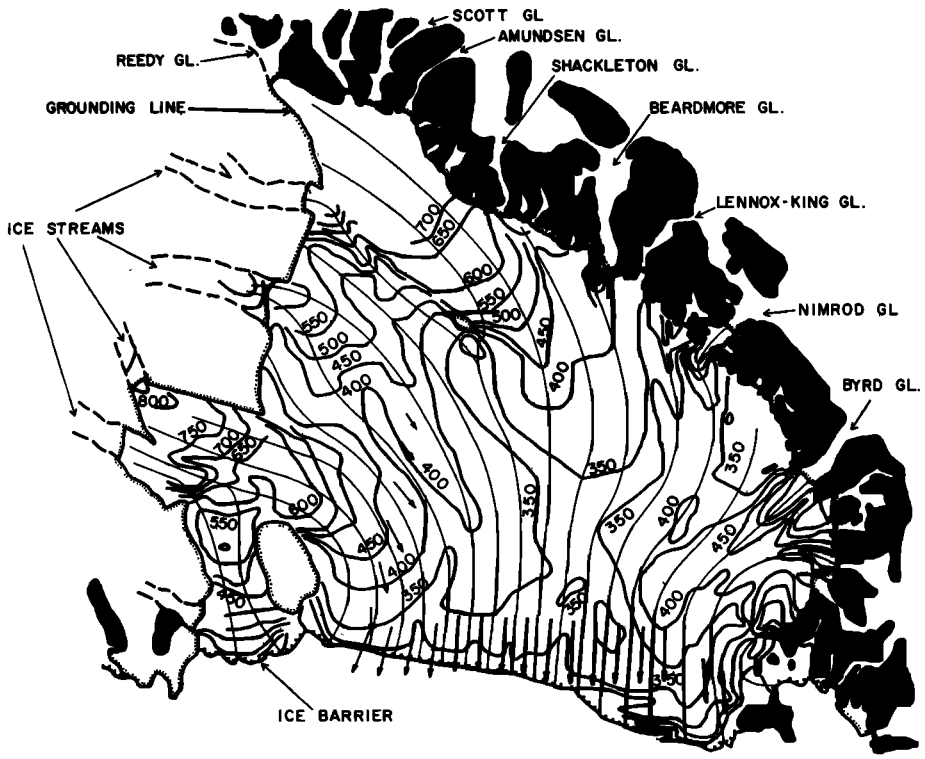

Fig. 8. Detailed flow of the Ross ice shelf. Shown are (1) the major west antarctic ice streams and east antarctic outlet glaciers, (2) selected absolute velocity vectors shown as arrows on the RISS traverse, (3) Ross ice shelf thickness contours at 50-meter intervals from the SPRI-NSF radio echo flights, (4) ice flowlines drawn as thin lines parallel to the absolute velocity vectors and generally normal to the ice thickness contours. (Modified from the SPRI-NSF Ross Ice Shelf Map [1972].)

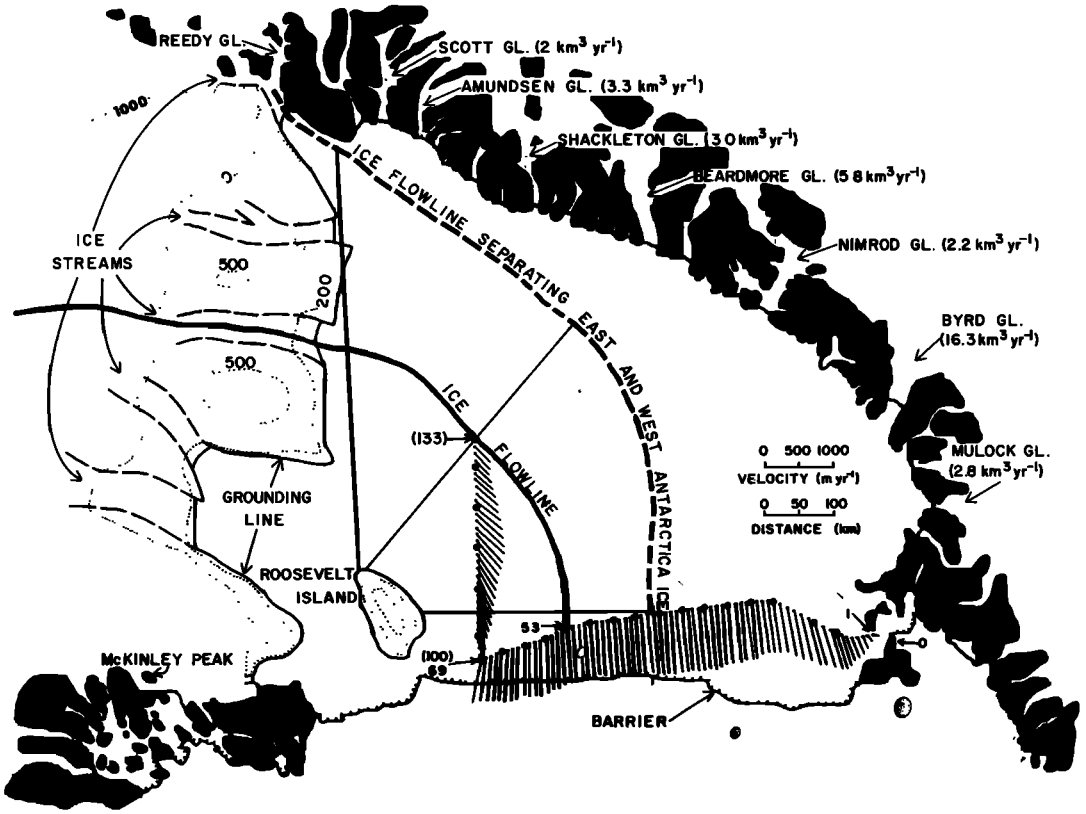

Fig. 9. General flow of the Ross ice shelf. Shown are (1) major ice streams from Marie Byrd Land, including the depression of the ice sheet surface above these ice streams as shown by the 200-meter and 500-meter elevation contours (the mass balance ice inputs from these ice streams are given in Table 2), (2) the major outlet glaciers from East Antarctica, including the mountainous areas projecting through the ice sheet as shown by blackened areas (the ice inputs from these outlet glaciers are given in parentheses), (3) the centerline of ice stream A in Figure 2, which separates east antarctic ice from west antarctic ice (heavy dashed line), (4) the ice flowline in Figures 2, 3, and 4, that joins ice stream C in Figure 2 (heavy solid line), (5) convergence of ice flow from the grounding line of Marie Byrd Land to the barrier of the Ross ice shelf (thin straight lines connecting Roosevelt Island to ice stream A and normal to the flowline of ice stream C), (6) absolute velocity vectors along the E-W legs (stations 0–69) and N-S legs (stations 100–133 in parentheses) of the RISS (thin straight lines connected to dots), and (7) RISS stations where the basal melting rates presented in Figure 10 were calculated (circled dots along the RISS traverse). (From *Giovinetto and Zumberge* [1968]; *Dorrer et al.* [1969]; *Robin et al.* [1970]; and J. H. Zumberge, unpublished data, 1971.)

Hence increasing sea level accounts for only a minor part of the apparent retreat rate of the grounding line, and the major cause of retreat must be due to an inherent instability in the west antarctic ice sheet that is largely independent of known sea level changes.

A possible consequence of extensive basal melting along the Siple Coast grounding line but concentrated under the major ice streams is retreat of the grounding line up the ice streams. This also would eventually cause a retreat of the grounding line between ice streams, such as appears to have happened between ice streams D and E in Figure 2. If a local ice dome exists between ice streams, such as the one between ice streams C and D in Figure 2, it will become a rise or island on the ice shelf when the flanking ice streams become ungrounded and merge. Roosevelt Island was probably an ice dome that became isolated

when the grounding line retreated around the high ground under the dome until ice streams D and E finally merged.

An estimate of the recent retreat velocity of the Marie Byrd Land grounding line of the Ross ice shelf is possible from a comparison of calculated and measured ice thickness changes at RISS station 133. If independent mechanisms contributing to Δh are additive, the calculated difference in ice thickness between the grounding line and RISS station 133 is

$$\Delta h = \Delta h_e + \Delta h_c + \Delta h_a \qquad (12)$$

where Δh_e, Δh_c, and Δh_a are the respective ice thickness changes caused by extension from gravity thinning, compression from lateral convergence, and mass balance caused by a net accumulation or ablation. The conservation of volume principle is used to calculate Δh_e from ϵ_x^* and the values of u, h, and x listed in Table 3. It can be shown [*Hughes*, 1972*c*] that lateral compression ϵ_y causes only a minor extension ϵ_z so that $\Delta h_c \cong 0$. Since a averaged for the top and bottom surfaces is unknown between the grounding line and RISS station 133, it will be assumed that $a \cong 0$ so that $\Delta h_a \cong 0$. Therefore, as a first approximation $\Delta h \cong \Delta h_e$. Since ice shelf thinning over hundreds of years is being considered, the strains involved are large and it is necessary to use true strains e_{ij} in place of engineering strains ϵ_{ij}. From conservation of volume, letting single primed values refer to the Siple Coast grounding line and double-primed values refer to RISS station 133

$$e_z = -e_x - e_y \qquad (13a)$$

$$\ln(\epsilon_z + 1) = -\ln(\epsilon_x + 1) - \ln(\epsilon_y + 1) \qquad (13b)$$

$$\ln\left[\frac{h'' - h'}{h'} + 1\right] = -\ln\left[\frac{\epsilon_x^*(x'' - x')}{(u'' + u')/2} + 1\right] - \ln\left[\frac{\Delta y'' - \Delta y'}{\Delta y'} + 1\right] \qquad (13c)$$

$$\ln\left[\frac{h''}{h'}\right] = -\ln\left[\epsilon_x^*\left(\frac{\Delta x}{\langle u\rangle}\right) + 1\right] - \ln\left[\frac{\Delta y''}{\Delta y'}\right] \qquad (13d)$$

where $\langle u\rangle = \frac{1}{2}(u'' + u')$.

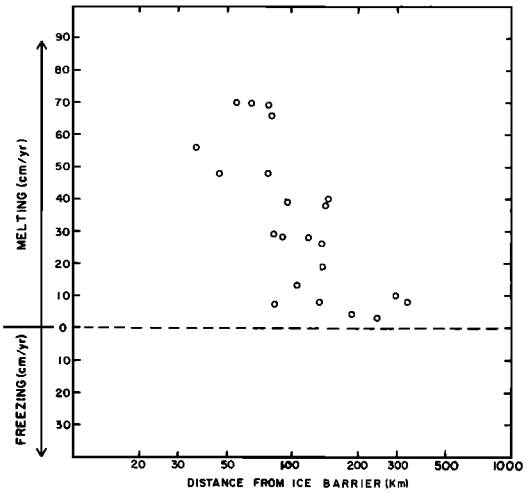

Fig. 10. Basal melting rates under the Ross ice shelf calculated at each of the RISS stations circled in Figure 9 (J. H. Zumberge, unpublished data, 1971).

Values of $\langle u\rangle$ and ϵ_x^* can only be estimated for ice stream C between the grounding line and RISS station 133, because u' must be estimated from the mass balance for Marie Byrd Land assuming no basal melting or freezing (Table 2) and ϵ_x^* must be estimated from theoretical spreading rates [*Hughes*, 1972*c*]. However the uncertainties in $\langle u\rangle$ and ϵ_x^* are compensating, and using the x, h, and u values in Table 3 to solve (13*d*) gives $h'' \cong 275$ meters for $n = 1.5$ and $h'' \cong 203$ meters for $n = 3$ [*Hughes*, 1972*c*]. Averaging these values gives $\Delta h = -421 \pm 36$ meters compared to $\Delta h = -180$ meters from Table 3. This discrepancy is so large that it can only be explained if, over at least the past $\Delta x/u'' = 880$ years, there has been a large positive mass balance or if the grounding line has been retreating.

The first explanation requires that $a > 0$ so that $\Delta h_a > 0$ in (12). In fact, over the last millenium $a = [(421 \pm 36 \text{ meters}) - (180 \text{ meters})]/[880 \text{ years}] = 0.27 \pm 0.04 \text{ m yr}^{-1}$, and using the present accumulation rate of $a_t = 0.14 \pm 0.05 \text{ m yr}^{-1}$ requires a basal freezing rate averaging $a_b = 0.13 \pm 0.09 \text{ m yr}^{-1}$. However, no sea ice layer has been detected by radio echo sounding; in fact, substantial basal melting is expected for this part of the flowline in Figure 9. This explanation therefore seems unlikely.

The second explanation requires that 880 years ago the ice thickness at the present grounding line was $h' = \Delta h + h'' = (421 \pm 36\text{m}) + (660 \text{ meters}) = 1081 \pm 36$ meters. For sea floor depths under the Ross ice shelf reported by *Crary et al.* [1962*a*, *b*] and plotted in Figure 4, an ice cover this thick at the present grounding line would require a grounding line further downstream in the vicinity of RISS station 133. Hence the grounding line has retreated about 300 km during the last millenium at an average rate of about 300 m yr^{-1}. If maintained, this retreat rate would unground the west antarctic ice sheet in about 6000 years, raising sea level over 4 meters worldwide. However, this fast retreat rate may be temporary. For example, if the grounding line retreat had averaged 70 m yr^{-1} over the last 10,000 years, as expected, then 300 m yr^{-1} for the last 1000 years requires 44 m yr^{-1} for the preceding 9000 years and this would be the usual rate. A recent surge would further reduce the usual retreat rate, although equations 13 are not derived for such conditions.

One condition for a sudden rapid retreat of the grounding line is illustrated in Figure 4. The dotted flotation line shows the elevation of sea level necessary to unground the Marie Byrd Land ice cover. A net negative mass balance causes a general lowering and a draining water pocket under one of the 'pseudo ice shelves' shown in Figure 4 causes a local lowering [*Robin et al.*, 1970*b*]. Since the slope α of the flotation line is the average of the top and bottom surface slopes of the ice cover, local sectors may exist where $\alpha \geq 0$ in the downstream direction. This condition is especially probable when a deep water pocket is being drained, because the top surface slope is already low and the bottom surface slope is increasing. Drainage of water pockets, therefore, tends to both lower the flotation line and increase its slope in the positive sense. The lowering is a general phenomenon because it includes basal ablation in the drainage channel as well as collapse of the water pocket. The slope increase is a regional phenomenon confined mainly to the ice cover overlying a collapsing water pocket. When the general lowering and regional slope increase combine so that suddenly $\alpha \geq 0$ from the grounding line to a point behind the grounding line (possibly determined by the length of a draining water pocket), the grounding line should immediately recede to that point. This could upset the local flow dynamics enough to cause a grounding line surge of the major ice stream involved. Such a situation may explain the unusually rapid recent retreat rate of the grounding line of ice stream C predicted by (12) and (13), provided the recent retreat did in fact occur. If so, the former grounding line may have been at a postulated grounding point, causing the fork in ice stream C shown in Figure 2.

CONCLUSIONS

A polar ice sheet grounded below sea level may be inherently unstable due to its capacity to respond drastically to moderate climatic warming, its ability to trap brine pockets during grounding, and its optimum probability for thermal convection. Any one of these instability features might result in disintegration of the ice sheet at a much more rapid rate than would seem possible for a similar ice sheet grounded above sea level. Hence, the west antarctic ice sheet is expected to be much less stable than the east antarctic ice sheet, and this seems to be verified by the limited data available. These data suggest that the west antarctic ice sheet has followed the general trend toward disintegration experienced by other continental ice sheets toward the end of the last Pleistocene ice age. Disintegration of these ice sheets was occasionally checked by temporary advances, and this pattern also seems to hold for the west antarctic ice sheet. The reduction of ice elevation in central Marie Byrd Land, on outlet glaciers through the Transantarctic Mountains, and on various glaciers in the Dry Valleys is the only direct evidence that disintegration is presently continuing.

The question of whether a surge of the antarctic ice sheet initiates a chain of events culminating in a global ice age is unresolved. However, this paper has tried to show that instability features possibly triggering a surge are most likely in the west antarctic ice sheet. These features could best be examined in detail by making a comprehensive field investigation of a major ice stream from its origin on the Marie Byrd Land ice divide to its terminus at the Ross ice shelf barrier. Ice stream C in

Figure 2 is recommended for this investigation. Its upper end lies in the region where thermal instability is most likely and here diapiric activity may have been detected. Its central portion degenerates into a number of pseudo ice shelves that may be related to trapped or draining brine pockets. Its grounding line portion is perhaps the best site for studying the dynamics of disintegration, because here the grounded and floating portions of the ice sheet interact most strongly and here most ice and basal meltwater are discharged from the grounded ice cover. Its floating portion may be the surged front of the ice sheet, with the outline of damped ice streams preserved by the ice thickness contours. The Ross Sea floor beyond the present ice terminus holds a record of past ice stream history if the long narrow channels in the sea floor were eroded by ice streams when the ice sheet was grounded in this region.

APPENDIX

The following is an estimate of the wet-base ice sheet elevation needed to deposit the Sirius Formation.

The Sirius Formation is a basal moraine deposited in a wet environment [*Mercer*, 1968*a*, 1972; *Mayewski*, 1972, 1973]. Therefore the base of the ice sheet that deposited the moraine was at the pressure melting point and had a basal debris layer that absorbed or deposited till, perhaps in the manner proposed by *Weertman* [1966] in which material is deposited in the zone of basal ablation (melting) and absorbed in the zone of basal accumulation (freezing). For a wet-base ice sheet the melting zone is toward the center and the freezing zone is toward the periphery. Furthermore, melting tends to occur when the basal slope is positive and freezing tends to occur when the basal slope is negative, taking x to be horizontal and positive downstream, z to be vertical and positive upward, and the origin to be at the ice-bed interface [*Budd et al.*, 1970]. In the Ross Sea ice drainage basin, east antarctic basal ice originates in the vicinity of the subglacial Gamburtsev Mountains, descends to the floor of the Wilkes polar subglacial basin, and ascends to the outlet glaciers through the Transantarctic Mountains. Assuming an ancient wet-base ice sheet deposited the Sirius Formation when it retreated, the basal freezing zone where the basal debris was absorbed into the ice would extend from the floor of the Wilkes polar subglacial basin to the divide of the Transantarctic Mountains.

Heat is supplied to the base of an ice sheet by the geothermal flux and the friction of internal deformation. Near the center of an ice sheet, downstream flow is slow so little frictional heat is available. In this case the difference between the top surface temperature T_t and the bottom surface temperature T_b is [*Robin*, 1955]:

$$T_t - T_b = \frac{G}{C_v \kappa}\left(\frac{2H\kappa}{a_t}\right)^{1/2} \cdot \left[\operatorname{erf}\left\{\left(\frac{a_t}{2H\kappa}\right)^{1/2} z\right\}\right]_z^h \qquad (14)$$

where $G = 1.6 \times 10^{11}$ erg cm^{-2} yr^{-1} is the mean geothermal heat flux for continental cratons, $C_v = 1.88 \times 10^9$ erg cm^{-3} °C^{-1} is the heat capacity of ice at constant volume, $\kappa = 1.18 \times 10^{-2}$ cm^2 sec^{-1} is the thermometric diffusivity of ice, H is ice thickness at the center, and a_t is the top surface accumulation rate in ice equivalent.

Over the polar plateau of East Antarctica, $a_t \cong 3.5$ cm yr^{-1} and consists mainly of hoarfrost and ice crystals descending from the troposphere [*Schwerdtfeger*, 1969; *Bull*, 1971]. These sources of precipitation are relatively independent of the ice sheet elevation, so past and present accumulation rates over the interior of East Antarctica should be about the same. At present, for interior East Antarctica $T_t \cong -55$°C, $H \cong 3.4$ km, and the bed elevation averages close to sea level. Using an adiabatic lapse rate of −1°C per +100 meters elevation and an isostatic bed depression of one-third the ice thickness [*Weertman*, 1961], (14) gives $T_b = T_M = -3$°C when $T_t \cong -60$°C, $H \cong 4.3$ km, and the ice sheet surface elevation is about 4.0 km. Hence, the Robin analysis for the interior of a polar ice sheet predicts that the maximum elevation of an ancient wet-base antarctic ice sheet is 4 km.

Assume the flowlines shown in Figure 1 were about the same when the postulated ancient wet-base antarctic ice sheet extended to the edge of the continental shelf and retreated to deposit the Sirius Formation. In (3) take x' and

TABLE 4. Estimated Elevation of an Ancient Wet-Base Ice Sheet above the Sirius Formation

Location of Sirius Formation[a]	Present Till Elevation,[a] meters	x'/L (Equation 3)	h'/H (Equation 3)	Former Ice Sheet Elevation, meters
Tillite Spur	2600	0.500	0.840	3360
Mt. Blackburn	3000	0.460	0.860	3440
Mt. Saltonstall	2200	0.430	0.875	3500
Mt. Innis-Taylor	2200	0.430	0.875	3500
Mt. Wisting	2000	0.430	0.875	3500
Roberts Massif	2100	0.460	0.860	3440
Mt. Block	2700	0.460	0.860	3440
Dismal Buttress	2300	0.470	0.855	3420
Half-Century Nunatak	2600	0.470	0.855	3420
Bennett Platform	2150	0.470	0.855	3420
Mt. Roth	800	0.500	0.840	3360
Otway Massif	2400	0.470	0.855	3420
Dominion Range	2200	0.450	0.865	3460
Mt. Deakin	2800	0.480	0.850	3400
Mt. Sirius	2300	0.450	0.865	3460
Mt. Feather	2800	0.700	0.700	2800
Shapeless Mountain	2400	0.750	0.660	2640
Carapace Nunatak	2000	0.790	0.615	2460
Coombs Hills	1900	0.810	0.595	2380
Allan Nunatak	1750	0.820	0.580	2320

[a] *Mayewski* [1972].

h' as flowline surface coordinates above each of the twenty Sirius Formation sites listed by *Mayewski* [1972] for the Transantarctic Mountains, L as the distance along flowlines from the center of the ice sheet to the edge of the continental shelf, $H = 4$ km as the wet-base ice sheet central thickness above sea level, and $n = 3$. Table 4 then gives the estimated ancient wet-base ice sheet elevations at the twenty known deposits of the Sirius Formation. Note that former ice sheet elevation minus present till elevation does not give ice thickness above the Sirius Formation sites, since reduction of the ice cover has been accompanied by isostatic uplift.

Acknowledgments. The merits of this paper spring from the generous cooperation of my colleagues, who provided both original data and mental stimulation. In particular I thank Dr. James Zumberge for making available his analysis of basal melting rates along the RISS on which Figure 10 is based, Dr. Ian Whillans for letting me quote from his dissertation analysis of the BSSN data, Dr. Gilbert Dewart for his BSSN ice thickness data, and Mr. Henry Brecher for his BSSN snow accumulation data, on which Figure 6 is based, and Dr. Paul Mayewski for sharing the results of his glacial geology studies in the Transantarctic Mountains on which Figure 4 is based. I also thank Dr. John Mercer, Dr. Maurice McSaveney, and Mr. John Splettstoesser for many helpful discussions and for directing me to important reference material.

This article is contribution 245 of the Institute of Polar Studies, Ohio State University, Columbus, Ohio 43210.

REFERENCES

Anderson, J. B., The marine geology of the Weddell Sea, Ph.D. dissertation, Fla. State Univ., Tallahassee, 1972.

Angino, E., and L. Lepley, Ross Sea, in *The Encyclopedia of Oceanography*, edited by R. Fairbridge, pp. 751–753, Reinhold, New York, 1966.

Auer, V., The Quaternary history of Fuego-Patagonia, *Proc. Roy. Soc., Ser. B, 152*, 507–516, 1960.

Bender, J. A., and A. J. Gow, Deep drilling in Antarctica, *Int. Ass. Sci. Hydrol. Publ. 55*, 132–141, 1961.

Bennett, H. F., A gravity and magnetic survey of the Ross ice shelf area, Antarctica, *Res. Rep. Ser. 64-3*, Geophysical and Polar Res. Center, Univ. of Wis., Madison, 1964.

Bentley, C. R., The structure of Antarctica and its ice cover, in *Research in Geophysics*, vol. 2, *Solid Earth and Interface Phenomena*, edited by H. Odishaw, pp. 335–389, MIT Press, Cambridge, Mass., 1964.

Bentley, C. R., Seismic anisotropy in West Antarctica, in *Antarctic Snow and Ice Studies II, Antarctic Res. Ser.*, vol. 16, edited by A. P. Crary, pp. 131–177, AGU, Washington, D.C., 1971.

Bentley, C. R., and F.-K. Chang, Geophysical exploration in Marie Byrd Land, Antarctica, in *Antarctic Snow and Ice Studies II, Antarctic Res. Ser.*, vol. 16, edited by A. P. Crary, pp. 1–38, AGU, Washington, D.C., 1971.

Brecher, H., Analysis of the Byrd Station strain net, Antarctica: Snow accumulation, *Rep. 48*, Ohio State Univ. Res. Found., Inst. of Polar Stud., Columbus, 1973.

Broecker, W. S., D. L. Thurber, J. Goddard, T. L. Ku, R. K. Matthews, and K. J. Mesolella, Milankovitch hypothesis supported by precise dat-

ing of coral reef and deep-sea sediments, *Science, 159*, 297–300, 1968.

Budd, W., The dynamics of ice masses, *Sci. Rep., Ser. A(IV), Publ. 108*, Aust. Nat. Antarctic Res. Exped., Melbourne, Australia, 1969.

Budd, W., D. Jenssen, and U. Radok, The extent of basal melting in Antarctica, *Polarforschung, 6*, 293–306, 1969 (publ. 1970).

Budd, W., Ice flow over bedrock perturbations, *J. Glaciol., 9*, 29–47, 1970.

Bull, C., Snow accumulation in Antarctica, in *Research in the Antarctic*, edited by L. Quam, pp. 367–421, Amer. Ass. for the Advan. of Sci., Washington, D.C., 1971.

Butkovich, T. R., and J. K. Landauer, The flow law for ice, *Int. Ass. Sci. Hydrol. Publ. 47*, 318–327, 1958.

Calkin, P. E., R. E. Behling, and C. Bull, Glacial history of Wright Valley, Southern Victoria Land, Antarctica, *Antarctic J., 5(1)*, 22–27, 1970.

Cameron, R. L., and R. P. Goldthwait, The US-IGY contribution to Antarctic glaciology, *Int. Ass. of Sci. Hydrol. Publ. 55*, 7–13, 1961.

Chriss, T., and L. A. Frakes, Glacial marine sedimentation in the Ross Sea, in *Antarctic Geology and Geophysics*, edited by R. J. Adie, pp. 747–762, Universitetsforlaget, Oslo, Norway, 1972.

Craddock, C., J. J. Anderson, and G. F. Webers, Geologic outline of the Ellsworth Mountains, in *Antarctic Geology*, edited by R. J. Adie, pp. 155–170, John Wiley, New York, 1964.

Crary, A. P., Glaciological regime at Little America Station, Antarctica, *J. Geophys. Res., 66*, 871–878, 1961.

Crary, A. P. (Ed.), *Antarctic Snow and Ice Studies II, Antarctic Res. Ser.*, vol. 16, AGU, Washington, D.C., 1971.

Crary, A. P., E. S. Robinson, H. F. Bennett, and W. Boyd, Glaciological regime of the Ross ice shelf, *J. Geophys. Res., 67*, 2791–2807, 1962*a*.

Crary, A. P., E. S. Robinson, H. F. Bennett, and W. Boyd, Glaciological studies of the Ross ice shelf, Antarctica, 1957–1960, *Glaciology, IGY Glaciol. Rep. 6*, IGY World Data Center A, Amer. Geogr. Soc., New York, 1962*b*.

Denton, G. H., R. L. Armstrong, and M. Stuiver, Late Cenozoic glaciation in Antarctica: The record in the McMurdo Sound region, *Antarctic J., 5(1)*, 15–21, 1970.

Denton, G. H., R. L. Armstrong, and M. Stuiver, The Late Cenozoic glacial history of Antarctica, in *The Late Cenozoic Glacial Ages*, edited by Karl K. Turekian, pp. 267–306, Yale University Press, New London, Conn., 1971.

Dewart, G., Analysis of the Byrd Station strain net, Antarctica: Geophysical investigations, *Rep. 48*, Inst. of Polar Stud., Ohio State Univ. Res. Found., Columbus, Ohio, 1973.

Dorrer, E., Movement determination of the Ross ice shelf, Antarctica, *Int. Ass. Sci. Hydrol. Publ. 86*, 467–471, 1970.

Dorrer, E., W. Hofmann, and W. Seufert, Geodetic results of the Ross ice shelf survey expeditions, 1962–63 and 1965–66, *J. Glaciol., 8*, 67–90, 1969.

Doumani, G. A., Volcanoes of the Executive Committee Range, Byrd Land, in *Antarctic Geology*, edited by R. J. Adie, pp. 666–675, John Wiley, New York, 1964.

Evans, S., and G. deQ. Robin, Ice thickness measurements, by radio echo sounding, 1971–1972, *Antarctic J., 7*(4), 108–110, 1972.

Fillon, R. H., Extensive Late Cenozoic disconformity in the Ross Sea, Antarctica (abstract), *EOS Trans. AGU, 53*, 422, 1972.

Giovinetto, M. B., The drainage systems of Antarctica: Accumulation, *Antarctic Snow and Ice Studies, Antarctic Res. Ser.*, vol. 2, pp. 127–155, 1964.

Giovinetto, M. B., and J. H. Zumberge, The ice regime of the eastern part of the Ross ice shelf drainage system, *Int. Ass. Sci. Hydrol. Publ. 79*, 255–266, 1968.

Giovinetto, M. B., E. S. Robinson, and C. W. M. Swithinbank, The regime of the western part of the Ross ice shelf drainage system, *J. Glaciol., 6*, 55–68, 1966.

Glen, J. W., The creep of polycrystalline ice, *Proc. Roy. Soc., Ser. A, 228*, 519–538, 1955.

Gow, A. J., The inner structure of the Ross ice shelf at Little America 5, Antarctica, as revealed by deep core drilling, *Int. Ass. Sci. Hydrol. Publ. 61*, 272–284, 1963.

Gow, A. J., Preliminary results of studies of ice cores from the 2164 m deep drill hole, Byrd Station, Antarctica, *Int. Ass. Sci. Hydrol. Publ. 86*, 78–90, 1970.

Gow, A. J., H. T. Ueda, and D. E. Garfield, Antarctic ice sheet: Preliminary results of first corehole to bedrock, *Science, 161*, 1011–1013, 1968.

Haefeli, R., Contribution to the movement and the form of ice sheets in the Arctic and Antarctic, *J. Glaciol., 3*, 1133–1150, 1961.

Higashi, A., Mechanical properties of ice single crystals, in *Physics of Ice*, edited by N. Riehl, B. Bullemer, and H. Engelhardt, pp. 197–212, Plenum, New York, 1969.

Higashi, A., S. Koinuma, and S. Mae, Plastic yielding of ice single crystals, *Jap. J. Appl. Phys., 3*, 610–616, 1964.

Higashi, A., S. Koinuma, and S. Mae, Bending creep of ice single crystals, *Jap. J. Appl. Phys., 4*, 575–582, 1965.

Higashi, A., S. Mae, and A. Fukuda, Strength of ice single crystals in relation to the dislocation structure, *Trans. J. Inst. Met., 9*(suppl.), 784–789, 1968.

Houtz, R., and R. Meijer, Structure of the Ross sea shelf from profiler data, *J. Geophys. Res., 75*, 6592–6597, 1970.

Hughes, T., Convection in the Antarctic ice sheet leading to a surge of the ice sheet and possibly to a new ice age, *Science, 170*, 630–633, 1970.

Hughes, T., Convection in polar ice sheets as a model for convection in the earth's mantle, *J. Geophys. Res., 76*, 2628–2638, 1971.

Hughes, T., Derivation of the critical Rayleigh

number for convection in crystalline solids, *J. Appl. Phys., 43,* 2895–2896, 1972*a*.

Hughes, T., Thermal convection in polar ice sheets related to the various empirical flow laws of ice, *Geophys. J. Roy. Astron. Soc., 27,* 215–229, 1972*b*.

Hughes, T., Scientific justification, Ice Streamline Coop. Antarctic Proj., *ISCAP Bull. 1,* Ohio State Univ., Inst. of Polar Stud., Columbus, 1972*c*.

Itagaki, K., Self-diffusion in single crystals of ice, *J. Phys. Soc. Jap., 19,* 1081, 1964.

Jacobs, S. S., A. F. Amos, and P. M. Bruchhausen, Ross Sea oceanography and Antarctic bottom water formation, *Deep Sea Res., 17,* 935–962, 1970.

Jelgersma, S., Sea-level changes during the last 10,000 years, in *World Climate from 8000 to 0 B.C.*, edited by J. S. Sawyer, pp. 54–69, Royal Meteorological Society, London, 1966.

Johnsen, S. J., W. Dansgaard, H. B. Clausen, and C. C. Langway, Jr., Oxygen isotope profiles through the Antarctic and Greenland ice sheets, *Nature, 235,* 429–434, 1972. (Also, Corrigendum, *Nature, 236,* 249, 1972.)

LeMasurier, W. E., Volcanic record of Cenozoic glacial history of Marie Byrd Land, in *Antarctic Geology and Geophysics,* edited by R. J. Adie, pp. 251–259, Universitetsforlaget, Oslo, Norway, 1972.

Map Sheet 13: Antarctica, Amer. Geogr. Soc., New York, 1970.

Mayewski, P. A., Glacial geology near McMurdo Sound and comparison with the central Transantarctic Mountains, *Antarctic J., 7*(4), 103–106, 1972.

Mayewski, P. A., The glacial geology and Late Cenozoic history of the Transantarctic Mountains, Ph.D. dissertation, Ohio State Univ., Columbus, 1973.

McSaveney, M., and E. McSaveney, A re-appraisal of the Pecten glacial episode, Wright Valley, Antarctica, *Antarctic J., 7*(6), 235–240, 1972.

Mellor, M. (Ed.), *Antarctic Snow and Ice Studies, Antarctic Res. Ser.,* vol. 2, AGU, Washington, D.C., 1964.

Mercer, J. H., Glacial geology of the Reedy glacier area, Antarctica, *Bull. Geol. Soc. Amer., 79,* 471–486, 1968*a*.

Mercer, J. H., Antarctic ice and Sangamon sea level, *Int. Ass. Sci. Hydrol. Publ. 79,* 217–225, 1968*b*.

Mercer, J. H., Some observations on the glacial geology of the Beardmore glacier area, in *Antarctic Geology and Geophysics,* edited by R. J. Adie, pp. 427–433, Universitetsforlaget, Oslo, Norway, 1972.

Mercer, J. H., Cainozoic temperature trends in the southern hemisphere: Antarctic and Andean glacial evidence, in *Palaeoecology of Africa and of the Surrounding Islands and Antarctica,* vol. 3, edited by E. M. van Zinderen Bakker, Balkema, Cape Town, in press, 1973.

Nichols, R. L., Coastal geomorprology, McMurdo Sound, Antarctica: Preliminary report, *IGY Glaciol. Rep. 4,* IGY World Data Center A, Amer. Geogr. Soc., New York, 1961.

Nye, J. F., The flow law of ice from measurements in glacier tunnels, laboratory experiments, and the Jungfraufirn borehole experiment, *Proc. Roy. Soc., Ser. A, 218,* 477–489, 1953.

Nye, J. F., The distribution of stress and velocity in glaciers and ice sheets, *Proc. Roy. Soc., Ser. A, 239,* 113–133, 1957.

Nye, J. F., The motion of ice sheets and glaciers, *J. Glaciol., 3,* 493–507, 1959.

Nye, J. F., Plasticity solution for a glacier snout, *J. Glaciol., 6,* 695–715, 1967.

Péwé, T. L., Multiple glaciation in the McMurdo Sound region, Antarctica: A progress report, *J. Geol., 68,* 498–513, 1960.

Redfield, A. C., Postglacial change in sea level in the western North Atlantic Ocean, *Science, 157,* 687–692, 1967.

Rigsby, G. P., Effect of hydrostatic pressure on velocity of shear deformation of single ice crystals, *J. Glaciol., 3,* 273–278, 1958.

Robin, G. deQ., Ice movement and temperature distribution in glaciers and ice sheets, *J. Glaciol., 2,* 523–533, 1955.

Robin, G. deQ., Commentary on paper by Giovinetto and Zumberge, *Int. Ass. Sci. Hydrol. Publ. 79,* 265–266, 1968.

Robin, G. deQ., S. Evans, D. J. Drewry, C. H. Harrison, and D. L. Petrie, Radio echo sounding of the Antarctic ice sheet, *Antarctic J., 5*(6), 229–232, 1970*a*.

Robin, G. deQ., C. W. M. Swithinbank, and B. M. E. Smith, Radio echo exploration of the Antarctic ice sheet, *Int. Ass. Sci. Hydrol. Publ. 86,* 97–115, 1970*b*.

Robinson, E. S., Geological structure of the Transantarctic Mountains and adjacent ice-covered areas, Antarctica, Ph.D. dissertation, Univ. of Wis., Madison, 1964.

Rutford, R. H., C. Craddock, C. M. White, and R. L. Armstrong, Tertiary glaciation in the Jones Mountains, in *Antarctic Geology and Geophysics,* edited by R. J. Adie, pp. 239–243, Universitetsforlaget, Oslo, Norway, 1972.

Scholl, D. W., and M. Stuiver, Recent submergence of southern Florida: A comparison with adjacent coasts and other eustatic data, *Bull. Geol. Soc. Amer., 78,* 437–454, 1967.

Scholl, D. W., F. C. Craighead, Sr., and M. Stuiver, Florida submergence curve revised: Its relation to coastal sedimentation rates, *Science, 163,* 562–564, 1969.

Schwerdtfeger, W., Ice crystal precipitation on the Antarctic plateau, *Antarctic J., 4*(5), 221–222, 1969.

Shepard, F. P., Thirty-five thousand years of sea level, in *Essays in Marine Geology in Honor of K. O. Emery,* edited by T. Clements, University of Southern California Press, Los Angeles, 1–10, 1963.

SPRI-NSF Ross Ice Shelf Map, U.S. Geol. Surv., Washington, D.C., 1972.

Thiel, E., and N. A. Ostenso, The contact of the Ross ice shelf with the continental ice sheet, Antarctica, *J. Glaciol., 3,* 823–832, 1961.

Thomas, R. H., and P. H. Coslett, Bottom melting of ice shelves and the mass balance of Antarctica, *Nature, 228,* 47–49, 1970.

Wade, F. A., Northeastern borderlands of the Ross Sea: Glaciological studies in King Edward VII Land and northwestern Marie Byrd Land, *Geogr. Rev., 27,* 584–597, 1937.

Webb, P. N., Paleontology of Late Tertiary-Quaternary sediments in Wright Valley, Antarctica, *Antarctic J.,* 7(4), 96–97, 1972.

Weertman, J., Deformation of floating ice shelves, *J. Glaciol., 3,* 38–42, 1957.

Weertman, J., Equilibrium profile of ice caps, *J. Glaciol., 3,* 953–964, 1961.

Weertman, J., Effect of a basal water layer on the dimensions of ice sheets, *J. Glaciol., 6,* 191–207, 1966.

Weertman, J., Dislocation climb theory of steady-state creep, *Trans. Amer. Soc. Met., 61,* 681–694, 1968.

Weertman, J., Water lubrication mechanism of glacier surges, *Can. J. Earth Sci., 6,* 929–942, 1969.

Weertman, J., General theory of water flow at the base of a glacier or ice sheet, *Rev. Geophys. Space Sci., 10,* 287–333, 1972*a*.

Weertman, J., Creep of ice, in *Proceedings of the International Symposium on the Physics and Chemistry of Ice,* Royal Society of Canada, Ottawa, in press, 1972*b*.

Whillans, I. M., Analysis of the Byrd Station strain net, Antarctica: State of equilibrium, *Rep. 48,* Ohio State Univ. Res. Found., Inst. of Polar Stud., Columbus, 1973*a*.

Whillans, I. M., State of equilibrium of the West Antarctic inland ice sheet, *Science, 182,* 476–479, 1973*b*.

Wilson, A. T., Origin of Ice Ages: An ice shelf theory for Pleistocene glaciation, *Nature, 201,* 147–149, 1964.

Zotikov, I. A., Bottom melting in the central zone of the ice shield on the Antarctic continent and its influence upon the present balance of the ice mass, *Int. Ass. Sci. Hydrol. Ann. Bull. 8*(1), 36–43, 1963.

Zumberge, J. H., Horizontal strain and absolute movement of the Ross ice shelf between Ross Island and Roosevelt Island, Antarctica, *Antarctic Snow and Ice Studies, Antarctic Res. Ser.,* vol. 2, 65–81, 1964.

(Received December 29, 1971;
revised January 30, 1973.)